

Fig. 3. (A) Morphological changes in HL60 and U937 cells treated with allicin. HL60 and U937 cells treated with allicin (5 or 20 μM , respectively) for 2 h were collected and washed with PBS. Cells were visualized by confocal microscopy (original magnification $\times 40$). (Upper panel) Nontreated cells (the diameter of 100 cells was measured). (Lower panel) Allicin-treated cells. (B) Immunoblot analysis of extracts (20 μg protein/lane) from allicin treated HL60 cells at various time of allicin (5 μM) treatment. The degrees of cytochrome *c* release into the cytosol and of caspase 9 and caspase 3 activation were assessed. β -Actin served as a control to the amount of loaded protein. The analysis of caspase 3, 9 and β -actin was done on the same blot after stripping. The data were obtained from one representative experiment (total of three independent experiments). (C) Staining of HL60 cells with MitoTracker Red CMXRos. HL60 cells treated with allicin (5 μM , 6 h) were collected, resuspended in fresh medium and were stained for 30 min with MitoTracker Red CMXRos (0.05 μM , 30 min). After washing twice with PBS, cells were examined by fluorescence microscopy (original magnification $\times 40$).

level after 18 h. The band of cleaved caspase 9 appeared at 24 h, reached a maximal intensity at 48 h and was still seen at 72 h. Cleaved caspase 3 appeared at 30 h, became intense at 48 h and did not fade after 72 h (data not shown). Cleaved caspase 8 was not observed in either cell line after allicin treatment (data not shown).

3.2.4. Impaired mitochondrial activity

Mitochondrial activity was monitored with the XTT assay in cells treated with allicin (5 and 20 μM for HL60 and U937, respectively) for 16 h (Fig. 4). Both cell lines behaved similarly, showing a residual mitochondrial activity $65 \pm 5\%$ in HL60 and $62 \pm 5\%$ in U937 cells. At this stage, the drop in

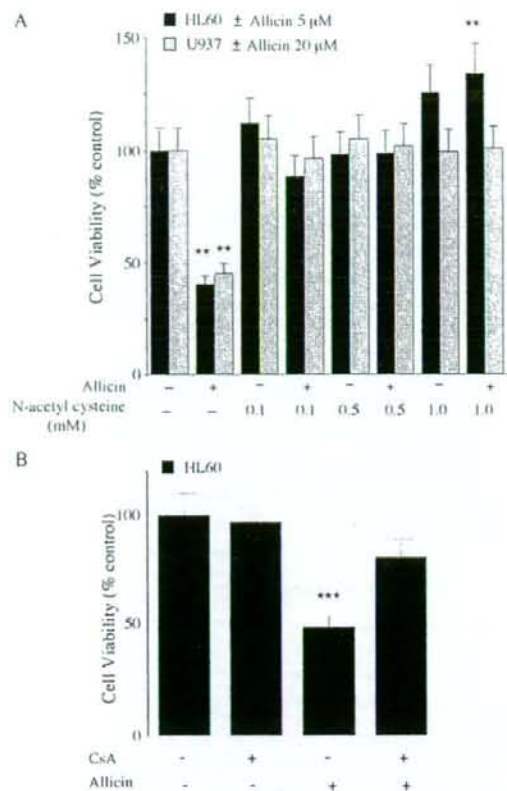


Fig. 4. (A) Allicin effect on cell viability in the absence or presence of *N*-acetyl cysteine. HL60 and U937 cells (100,000 cells/ml) were treated with allicin (5 or 20 μM, respectively) for 16 h, in the absence or presence of *N*-acetyl cysteine at 0.1, 0.5 and 1.0 mM. Cell viability was measured by the XTT assay after 3 h of incubation at 37°C with 5% CO₂. Means±S.D. of one experiment (*n*=6) are shown (total of three independent experiments). ***P*<.01 represents a significant difference from nontreated cells, based on one-way ANOVA followed by Dunnett's test. (B) Allicin effect on HL60 cell viability following a 1-h CsA (5 μM) pretreatment. HL60 cells (100,000 cells/ml) were treated with or without allicin (5 μM) for 16 h. Cell viability was measured by the XTT assay. Means±S.D. of one experiment (*n*=6) are shown (total of three independent experiments). ****P*<.001, represents significant difference compared with nontreated cells by one-way ANOVA followed by Bonferroni's multiple comparison test.

mitochondrial activity was not accompanied by a significant change in cell number. Such a change was observed only after 24 h. Nontreated HL60 cells proliferated at a higher rate than nontreated U937 cells. Although after 24 h nontreated HL60 cells exceeded nontreated U937 cells in number, mitochondrial activity (measured by XTT assay) in U937 cells (0.869±0.025 optical density [OD] units at 450 nm, *n*=6) was significantly higher than that in HL60 cells (0.498±0.073 OD units, *n*=6) (*P*<.001). These results indicate a higher battery of mitochondrial enzymes in U937 cells and

suggest a higher resistance to allicin. When cells were treated with allicin in the presence of NAC (0.1–1.0 mM), mitochondrial metabolic activity was not impaired, and the antiproliferative effect of allicin was precluded (Fig. 4A).

3.3. Allicin induces changes in mitochondrial membrane potential

Nontreated cells showed strong staining with MitoTracker Red CMXRos, indicating the negative membrane potential of the mitochondria and the accumulation of the lipophilic dye. In HL60 cells treated with allicin (5 μM, 6 h) the staining intensity decreased significantly, indicating changes in the mitochondrial membrane potential (Fig. 3C). Reduced mitochondrial staining in allicin-treated (20 μM) U937 cells occurred much slower; changes were observed 24 h after treatment, and the decline continued up to 40 h (data not shown).

A deeper insight into the involvement of mitochondrial permeability transition pore (mPTP) in the cytotoxicity of allicin was gained by using cyclosporine A (CsA), an inhibitor of adenine nucleotide translocator. HL60 cells were preincubated with 5 μM CsA for 1 h and then treated with allicin for 16 or 20 h. CsA inhibited the detrimental effects of allicin on cell viability as determined by the XTT assay (~80% residual viability for CsA pretreatment; ~50% for allicin alone). There was no significant difference between nontreated and CsA-treated cells (*P*>.05). No significant difference was found between CsA alone and CsA followed by allicin treated cells (*P*>.05) (Fig. 4B). CsA-pretreated cells were stained with Hoechst 33342 and MitoTracker Red CMXRos. CsA pretreatment prevented the nuclear condensation induced by treatment with allicin alone (Fig. 5). Mitochondrial staining also showed the preventive effect of CsA, whereby allicin-induced mitochondrial membrane depolarization was inhibited.

Fluorescence-activated cell sorting (FACS) analysis of HL60 cells treated with allicin (5 μM, 20 h) showed that 35.0% of the cells were apoptotic, whereas CsA pretreatment reduced the apoptotic fraction to 17.1% (*P*<.05). Cell arrest at G2 was increased in allicin-treated cells with or without CsA pretreatment 34.9% and 59.0%, respectively (Fig. 6). The fraction of HL60 cells at the G2 stage was 17.3% for nontreated cells and 18.9% for cells treated with CsA only (the difference is not significant).

3.4. Differences in GSH levels between HL60 and U937

GSH concentrations (nmol/total cell volume) in nontreated HL60 and U937 cells were almost the same: 3.4±0.48 mM and 3.7±0.55 mM, respectively. However, due to the differences in cell size between the two cell lines, analysis of GSH concentration expressed as a function of protein levels or cell numbers was also used. This analysis revealed significant differences between the GSH concentrations in the two cell lines. In nontreated HL60 cells, GSH concentration was 20.94±3.15 nmol/mg protein, and in nontreated U937 cells, 30.80±6.04 nmol/mg protein (*P*<.02). The

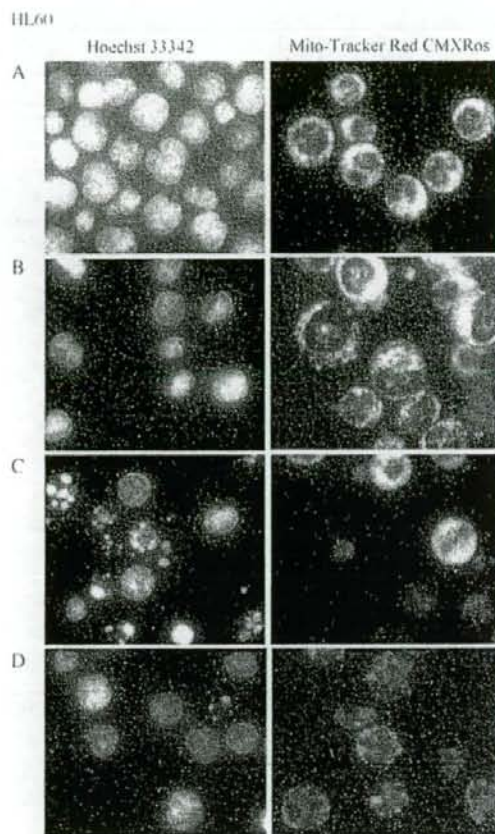


Fig. 5. Morphological effects of allicin on CsA pretreated HL60 cells. Cells ($200,000$ cells/ml) with or without CsA pretreatment ($5 \mu\text{M}$, 1h) were diluted and incubated in the presence or absence of allicin ($5 \mu\text{M}$) for 16 h. Cells were stained with Hoechst 33342 ($5 \mu\text{g/ml}$) or with Mito-Tracker Red CMXRos (50 nM) for 30 min. Cells were washed twice with PBS and examined by fluorescence microscopy. (A) HL60 nontreated. (B) CsA-treated. (C) Allicin-treated. (D) CsA- and allicin-treated.

difference was found to be even higher when cell numbers were considered, GSH concentration in HL60 cells was $3.7 \pm 0.56 \text{ nmol}/10^6$ cells whereas, in U937 cells, approximately twice as much [$7.7 \pm 1.08 \text{ nmol}/10^6$ cells ($P < .001$)].

3.5. Allicin-induced GSH depletion

Allicin treatment of HL60 cells caused a rapid decrease in GSH concentration, reaching its lowest point at about 30 min. A spontaneous recovery occurred, reaching the basal level of GSH (Fig. 7A). The highest GSH levels were observed in HL60 cells between 2–24 h after adding allicin. In allicin-treated U937 cells, a decrease in GSH levels to a minimal value occurred 2–4 h after treatment, and it was followed by a gradual increase to the basal GSH level (Fig. 7B).

3.6. Allicin-induced GSH depletion in the cells pretreated with BSO

In HL60 cells treated with BSO, an inhibitor of γ -glutamyl-cysteine synthetase (GGCS) (0.4 mM , 20 h) GSH levels decreased to $1.45 \pm 0.25 \text{ nmol}/10^6$ cells. No cell death was observed, but there was a slight decrease in the proliferation rate ($\times 1.7$ after 20 h as compared to $\times 2.1$ in

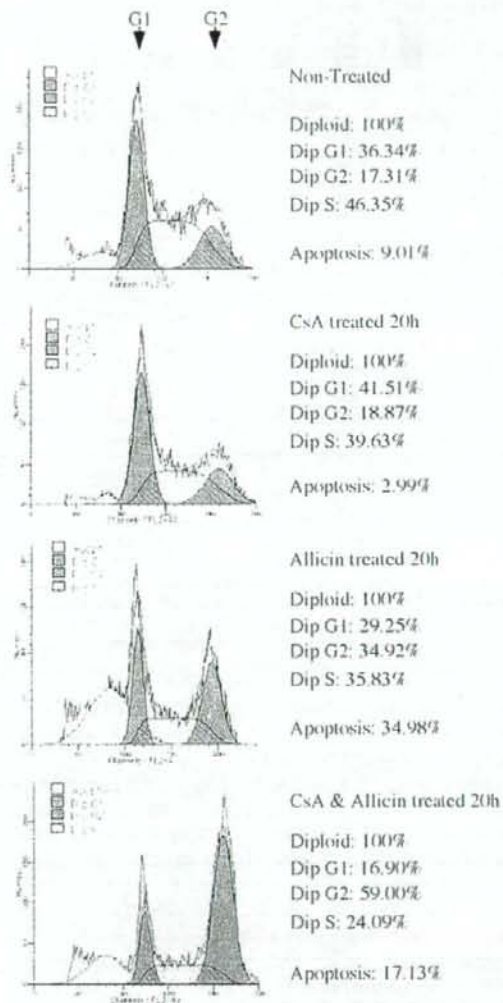


Fig. 6. Cell cycle analysis of allicin-treated HL60 cells. Cells ($200,000$ cells/ml, 1.5×10^6) with or without CsA pretreatment ($5 \mu\text{M}$, 1h) were diluted and incubated in absence or presence of allicin ($5 \mu\text{M}$) for 20 h. The cells were stained with propidium iodide in the presence of RNase A and Triton X-100, as described in Materials and methods. The data represent one experiment (total of three independent experiments).

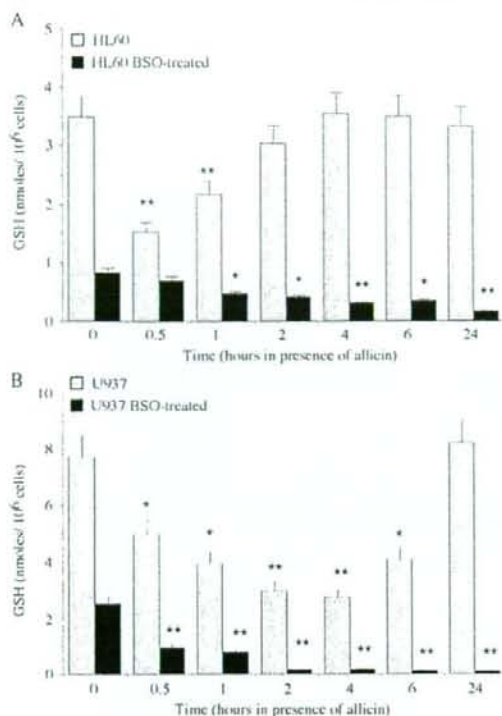


Fig. 7. Time-dependent decrease of GSH levels in alliin-treated HL60 and U937 cells after BSO pretreatment. Cells were pretreated with or without 0.4 mM BSO for 20 h. HL60 and U937 cell cultures were diluted to 100,000 cells/ml and were grown in the presence of alliin (5 and 20 μ M, respectively). At each time point, 30-ml samples were harvested and washed twice with PBS. Cell pellets were extracted with 5% metaphosphoric acid and analyzed for GSH content and protein concentration. Means \pm S.D. of one representative experiment (total of three independent experiments).

nontreated cells). Alliin (5 μ M) applied to HL60 cells pretreated with BSO (0.4 mM, 20 h) caused an additional GSH decrease to 0.65 ± 0.13 nmol/ 10^6 cells after 1 h (Fig. 7A, black column). There was no recovery of GSH as in the case of HL60 cells treated with alliin alone. In U937 cells pretreated with BSO (0.4 mM, 20 h), GSH levels decreased to 1.06 ± 0.14 nmol/ 10^6 cells. Also, in this case, no cell death was observed and cells were still proliferating. When BSO-pretreated U937 cells were incubated with alliin (20 μ M), GSH levels further decreased to 0.33 ± 0.08 nmol/ 10^6 cells within 2 h (Fig. 7B, black column). A high rate of cell death (60–80%) occurred in both cell lines 24 h after alliin was applied to the culture.

3.7. Reduction potential in alliin-treated cells

Since alliin-treated cells lost their spherical structure and their volume could not be calculated from diameter measurement, we had to use another parameter to calculate

changes in the intracellular reducing state resulting from fluctuations in 2GSH/GSSG ratios. Based on the assumption that 1-mg cell pellet is equivalent to 1 μ l of volume, cell pellets were weighed, and GSH molar concentration was calculated accordingly (GSH amount/cell weight). Therefore, calculated reduction potential represents only approximate values. The intracellular pH of HL60 cells is 7.0 [37], and the reported E_0 for this pH is -240 mV [27]. Using the above E_0 values, reducing potential (E_{GSH}) calculated for nontreated HL60 was -207 mV (GSH 3.42 ± 0.18 mM, GSSG 0.15 ± 0.023 mM) and for alliin-treated (0.5 h) -169 mV (GSH 1.4 ± 0.17 mM, GSSG 0.46 ± 0.082 mM). The intracellular pH of U937 cells is 7.04 [38] or 7.2 [39], and the

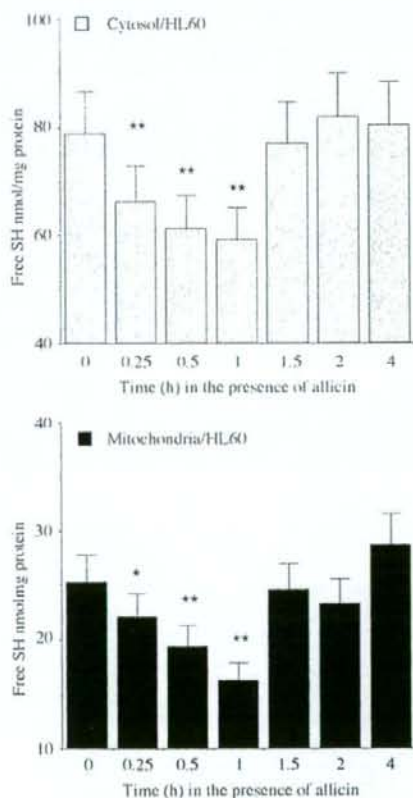


Fig. 8. Free SH contents in cytosolic and crude mitochondrial fractions from alliin-treated HL60 cells. Alliin (5 μ M) was added to cells growing at density of 100,000 cells/ml. At various intervals, 100-ml samples were harvested at 4°C, washed twice with PBS and stored at -80°C overnight. Cell fractionation was done as described in Materials and methods. Total free SH and protein concentrations were determined as described in Materials and methods. The SH content at various time intervals in the cytosol (upper panel) and in the crude mitochondrial fraction (lower panel) are shown. Means \pm S.D. of one representative experiment (total of three independent experiments) [40].

reported E_0 values are -240 mV or -252 mV, respectively. The calculated reducing potential values of nontreated U937 cells were -206 mV or -218 mV (GSH 3.7 ± 0.21 mM, GSSG 0.18 ± 0.040 mM), and for allicin-treated cells (2 h), -173 mV or -185 mV (GSH 1.54 ± 0.042 mM, GSSG 0.41 ± 0.021 mM). The values obtained for nontreated cells are characteristic of cells in proliferation/differentiation state, whereas those obtained after allicin treatment are typically obtained in the apoptotic state.

3.8. Free SH in the cytosolic and mitochondrial fractions of HL60 cells

Total free SH concentrations were determined in the cytosol and in the crude mitochondrial fractions prepared from allicin-treated HL60 cells. The decrease in free SH in the cytosol (Fig. 8, upper panel) was accompanied by a decrease of free SH in the mitochondria (Fig. 8, lower panel). Since mitochondrial GSH is supplied from the cytoplasm and upon allicin treatment it was depleted in both cellular compartments, it was followed by a substantial decrease in the cell-reducing potential. Consequently, depolarization of the mitochondrial membrane occurred and triggered a chain of apoptotic events leading to cell death.

4. Discussion

GSH, cysteine and accessible free SH groups of various proteins and peptides are rapidly oxidized by allicin to their respective allyl-SS derivatives [19,22]. The mixed disulfide formed is less active than allicin, yet it can easily react with free SH in thiol-disulfide exchange reactions, and produce, at the end of a series of reactions, the oxidized form of glutathione (GSSG), the oxidized form of cysteine (cystine) and glutathiolated S proteins. The leaving group (allyl-mercaptan) is volatile and rapidly disappears.

Glutathione is the major regulator of the thiol-disulfide redox state of living cells (reviewed in Refs. [29,41–43]). Alterations in cellular free thiols have already been described as a key event in the generation of apoptosis (reviewed in [44,45]).

In this study, allicin induced mitochondrial release of cytochrome *c*, activation of caspase 9 and 3 and DNA fragmentation in HL60 and U937 cell lines in a concentration- and time-dependent manner. GSH depletion had been shown to be associated with cell surface blebbing in hepatocytes [46]. Here, cell blebbing occurred in both HL60 and U937 cells treated with allicin. The rate of free SH depletion from the cytosol and the mitochondria was similar, indicating that allicin penetrated the mitochondria and the cell membrane equally well and reacted with free SH in both compartments. Allicin induced an initial drop in GSH levels that was followed by a regeneration process, occurring several hours after treatment. This may be due to decreased feedback inhibition of GSH biosynthetic enzymes such as GGCS by GSH [45]. Conversely, in BSO-pretreated cells,

there was no recovery of GSH after its allicin-induced depletion, as BSO is a direct inhibitor of GGCS. BSO pretreatment in allicin-treated U937 cells shortened the life span from 72 to 20 h, indicating that preliminary GSH depletion renders cells more sensitive to apoptosis. BSO-depleted GSH levels in U937 cells were, at this stage, similar to the inherent GSH level in HL60 cells and, hence, a similar degree of sensitivity to allicin.

Here, we have shown that allicin causes GSH depletion concomitantly in the cytosol and the mitochondria in HL60 cells. It is known that active GSH uptake by intact mitochondria occurs even at very low cytosolic GSH levels and that the rate of mitochondrial GSH depletion is much slower than that of the cytosol [47]. These are indications that mitochondria have more than one control mechanism to maintain GSH levels. Since BSO-induced depletion of GSH levels caused neither mitochondrial permeability transition nor apoptosis, it is likely that BSO treatment depletes GSH mainly from the cytosol, whereas allicin induced depletion of mitochondrial GSH trigger the apoptotic process. Moreover, CsA (mPTP inhibitor) pretreatment of HL60 cells inhibits allicin-induced mitochondrial permeability transition and cell death, corroborating the central role of mitochondria in the apoptotic process induced by allicin. Simultaneous addition of NAC and allicin to cells provided protection against the apoptotic damage. NAC sequestered the harmful activity by competing with GSH for the reaction with allicin.

The following allicin-induced apoptotic scenario can be deduced from this study: Allicin penetrates the cells and readily reacts with any exposed SH present in its vicinity. As GSH is the most abundant thiol molecule in the cytosol and the mitochondria, it is the main target for allicin reaction. The reaction with glutathione leads to an immediate change in the ratio GSH/GSSG. The increased concentration of GSSG and the depletion of GSH brings about a decrease in the cellular reduction potential state. Concomitantly, mitochondrial damage occurs, as is evident from changes in membrane potential, its decreased enzymatic activity and the release of cytochrome *c* to the cytosol. Upon its release, cytochrome *c* participates in the activation of the caspase 9, followed by activation of caspase 3.

Allicin induced cell cycle arrest at G2/M in HL60 cells (~35%). Upon CsA pretreatment, the percentage of cells at G2/M was even higher (~59%). After pretreatment of HL60 cells with CsA and 40-h incubation with allicin, there was no change in the number of viable cells, neither were there signs of cell breakage. By using CsA, it could be shown that the effect of allicin on cell cycle arrest was independent of its proapoptotic activity. The mechanism by which allicin induces G2/M cell arrest is not clear, but a clue may reside in its ability to inhibit microtubule assembly. It had been shown that microtubule assembly is disrupted by direct modification of tubulin SH groups [48–50] and that adding GSH to an in vitro microtubule assembly system disrupted by SH modification restores tubulin polymerization [51].

Here we have shown that, in allicin-treated cells, there is an increase in GSH synthesis. Therefore, cell cycle arrest would be expected to expire after tubulin recovery. However, the protracted G2/M phase induced by cyclosporine A and allicin suggests an additional modification of a critical pathway that needs an extended period to regenerate.

Allicin disappears from the medium very rapidly due to its penetration into the cells and its reaction with SH group. When applied to HL60 cells ($5 \mu\text{M}/10^5$ cells/ml) or to U937 cells ($20 \mu\text{M}/10^5$ cells/ml), it could not be detected in the medium after 2 h or 6–8 h in HL60 or U937 cells, respectively. The consumption of allicin within such a short time enables full activity of SH-dependent apoptotic enzymes such as the cysteine proteases and caspases 9 and 3 [52].

Cell sensitivity to allicin was shown to be dependent on the intracellular content of GSH. Since there is a significant difference in cell size between the two cell lines examined, comparing GSH amount/cell number showed that HL60 cells contained $3.7 \text{ nmol GSH}/10^6$ cells, whereas U937 cells contained $7.7 \text{ nmol GSH}/10^6$ cells. The differences in GSH intracellular content reflect differences in sensitivity to allicin. The higher the GSH, the less sensitive to allicin cells are, and the slower the apoptotic signs appear.

The allicin-induced decrease in GSH levels modulates the redox state of cells. In allicin-treated HL60 cells, the ratio of [GSH]/[GSSG or GSSA] changed within the first 30 min and the reducing potential reached -170 mV , whereas in U937 cells, it took 2 h to reach the same level. Such a high value is typical of the apoptotic state [27].

Since GSSA (the first main product of allicin reaction with GSH) is able to prevent the formation of free radicals [19], it is likely that the initial event inducing apoptosis does not occur via the generation of reactive oxygen species but rather through mitochondrial membrane depolarization or through a more finely tuned event mediated by protein modification upon creating a mixed disulfide [19,53]. Oxidative stress incurred by the accumulation of peroxides is a secondary event probably happening after the short-lived GSSA is eliminated from the cells.

It was reported that, in BSO-treated U937 cells, the depletion of GSH and the release of cytochrome *c* into the cytosol were counteracted by cell-repair systems involving nuclear factor κB and heat shock proteins [54]. Our results show that CsA and NAC prevented apoptosis induced by allicin. Taken together, the role allicin plays may be through direct modification of specific free SH in proteins, such as reside in apoptotic repair system, in the mPTP [55] or others.

Acknowledgment

We would like to thank Dr. A. Gross, Department of Biological Regulation, Weizmann Institute of Science for critical reading of the manuscript, and Mrs. Anna Gakamsky for her help in the statistical analysis.

References

- [1] Stoll A, Seebeck E. Chemical investigation on alliin, the specific principle of garlic. *Adv Enzymol* 1951;11:377–400.
- [2] Koch HP, Lawson LD. Garlic: the Science and therapeutic application of *Allium sativum* L. and related species. 2nd ed. Baltimore: Williams & Wilkins; 1996.
- [3] Elkayam A, Mirelman D, Peleg E, Wilchek M, Miron T, Rabinkov A, et al. The effects of allicin and enalapril in fructose-induced hyperinsulinemic hyperlipidemic hypertensive rats. *Am J Hypertens* 2001;14:377–81.
- [4] Eilat S, Oestraicher Y, Rabinkov A, Ohad D, Mirelman D, Battler A, et al. Alteration of lipid profile in hyperlipidemic rabbits by allicin, an active constituent of garlic. *Coron Artery Dis* 1995;6:985–90.
- [5] Abramovitz D, Gavri S, Harats D, Levkovitz H, Mirelman D, Miron T, et al. Allicin-induced decrease in formation of fatty streaks (atherosclerosis) in mice fed a cholesterol-rich diet. *Coron Artery Dis* 1999;10:515–9.
- [6] Gonen A, Harats D, Rabinkov A, Miron T, Mirelman D, Wilchek M, et al. The antiatherogenic effect of allicin: possible mode of action. *Pathobiology* 2005;72:325–34.
- [7] Lang A, Lahav M, Sakhrini E, Barshack I, Fiddler HH, Avidan B, et al. Allicin inhibits spontaneous and TNF- α induced secretion of proinflammatory cytokines and chemokines from intestinal epithelial cells. *Clin Nutr* 2004;23:1199–208.
- [8] Agarwal KC. Therapeutic actions of garlic constituents. *Med Res Rev* 1996;16:111–24.
- [9] Hirsch K, Danilenko M, Giat J, Miron T, Rabinkov A, Wilchek M, et al. Effect of purified allicin, the major ingredient of freshly crushed garlic, on cancer cell proliferation. *Nutr Cancer* 2000;38:245–54.
- [10] Knowles LM, Milner JA. Possible mechanism by which allyl sulfides suppress neoplastic cell proliferation. *J Nutr* 2001;131:1061S–6S.
- [11] Sun L, Wang X. Effects of allicin on both telomerase activity and apoptosis in gastric cancer SGC-7901 cells. *World J Gastroenterol* 2003;9:1930–4.
- [12] Oommen S, Anto RJ, Srinivas G, Karunagaran D. Allicin (from garlic) induces caspase-mediated apoptosis in cancer cells. *Eur J Pharmacol* 2004;485:97–103.
- [13] Park SY, Cho SJ, Kwon HC, Lee KR, Rhee DK, Pyo S. Caspase-independent cell death by allicin in human epithelial carcinoma cells: involvement of PKA. *Cancer Lett* 2005;224:123–32.
- [14] Antisperger DSM, Dirsch VM, Ferreira D, Su JL, Kuo ML, Vollmar AM. Ajoene-induced cell death in human promyelocytic leukemia cells does not require JNK but is amplified by the inhibition of ERK. *Oncogene* 2003;22:582–9.
- [15] Jin Z, El-Deiry WS. Overview of cell death signaling pathways. *Cancer Biol Ther* 2005;4:139–63.
- [16] Hsu YT, Wolter KG, Youle RJ. Cytosol-to-membrane redistribution of Bax and Bcl-X1 during apoptosis. *Proc Natl Acad Sci U S A* 1997;94:3668–72.
- [17] Wolter KG, Hsu YT, Smith A, Nechushtan A, Xi X, Youle RJ. Movement of Bax from the cytosol to mitochondria during apoptosis. *J Cell Biol* 1997;139:1281–92.
- [18] Miron T, Rabinkov A, Mirelman D, Wilchek M, Weiner L. The mode of action of allicin: its ready permeability through phospholipid membranes may contribute to its biological activity. *Biochim Biophys Acta* 2000;1463:20–30.
- [19] Rabinkov A, Miron T, Mirelman D, Wilchek M, Glozman S, Yavin E, et al. S-allylmercaptoglutathione: the reaction product of allicin with glutathione possesses SH-modifying and antioxidant properties. *Biochim Biophys Acta* 2000;1499:144–53.
- [20] Xiao H, Parkin KL. Antioxidant functions of selected allium thiosulfonates and S-alk(enyl)-L-cysteine sulfoxides. *J Agric Food Chem* 2002;50:2488–93.
- [21] Okada Y, Tanaka K, Sato E, Okajima H. Kinetic and mechanistic studies of allicin as an antioxidant. *Org Biomol Chem* 2006;4:4113–7.
- [22] Rabinkov A, Miron T, Konstantinovskii L, Wilchek M, Mirelman D, Weiner L. The mode of action of allicin: trapping of radicals and

- interaction with thiol containing proteins. *Biochim Biophys Acta* 1998;1379:233–44.
- [23] Freeman F, Koder Y. Garlic chemistry-stability of *S*-(2-propenyl) 2-propene-1-sulfinothioate (allicin) in blood, solvents, and simulated physiological fluids. *J Agric Food Chem* 1995;43:2332–8.
- [24] Lachmann G, Lorenz D, Radeck W, Steiper M. The pharmacokinetics of the S35 labeled garlic constituents alliin, allicin and vinylthiine. *Arzneimittelforschung* 1994;44:734–43.
- [25] Miron T, Mironchik M, Mirelman D, Wilchek M, Rabinkov A. Inhibition of tumor growth by a novel approach: in situ allicin generation using targeted alliinase delivery. *Mol Cancer Ther* 2003;2:1295–301.
- [26] Arditti F, Rabinkov A, Miron T, Reissner Y, Berrebi A, Wilchek M, et al. Apoptotic killing of B-chronic lymphocytic leukemia tumor cells by allicin generated in situ using a rituximab–alliinase conjugate. *Mol Cancer Ther* 2005;4:325–31.
- [27] Schafer FQ, Buettner GR. Redox environment of the cell as viewed through the redox state of the glutathione disulfide/glutathione couple. *Free Radic Biol Med* 2001;30:1191–212.
- [28] Jonas CR, Ziegler TR, Gu LH, Jones DP. Extracellular thiol/disulfide redox state affects proliferation rate in a human colon carcinoma (Caco2) cell line. *Free Radic Biol Med* 2002;33:1499–506.
- [29] Gilbert HF. Molecular and cellular aspects of thiol-disulfide exchange. *Adv Enzymol Relat Areas Mol Biol* 1990;63:69–172.
- [30] Stoll A, Seebeck E. Allium compounds V. The synthesis of natural alliin and its three optical active isomers. *Helv Chim Acta* 1951;34:481–7.
- [31] Miron T, SivaRaman H, Rabinkov A, Mirelman D, Wilchek M. A method for continuous production of allicin using immobilized alliinase. *Anal Biochem* 2006;351:152–4.
- [32] Nakagawa Y, Inuma M, Matsuura N, Yi K, Naoi M, Nakayama T, et al. A potent apoptosis-inducing activity of a sesquiterpene lactone, arucanolid, in HL60 cells: a crucial role of apoptosis-inducing factor. *J Pharmacol Sci* 2005;97:242–52.
- [33] Grinberg M, Schwarz M, Zaltsman Y, Eini T, Niv H, Pietrovski S, et al. Mitochondrial carrier homolog 2 is a target of tBID in cells signaled to die by tumor necrosis factor alpha. *Mol Cell Biol* 2005;25:4579–4590.
- [34] Gornall A, Bardawill C, David M. Determination of serum proteins by means of the biuret reaction. *J Biol Chem* 1949;177:751–66.
- [35] Anderson ME. Determination of glutathione and glutathione disulfide in biological samples. *Methods Enzymol* 1985;113:548–55.
- [36] Riddles PW, Blakeley RL, Zerner B. Ellman's reagent: 5,5'-dithiobis (2-nitrobenzoic acid) — a reexamination. *Anal Biochem* 1979;94:75–81.
- [37] Restrepo D, Kozody DJ, Spinelli LJ, Knauf PA. pH Homeostasis in promyelocytic leukemic HL60 cells. *J Gen Physiol* 1988;92:489–507.
- [38] Oehler R, Zellner M, Hefel B, Weingartmann G, Spittler A, Struse HM, et al. Influence of heat shock on cell volume regulation: protection from hypertonic challenge in a human monocyte cell line. *FASEB J* 1998;12:553–60.
- [39] Nilsson C, Kagedal K, Johansson U, Ollinger K. Analysis of cytosolic and lysosomal pH in apoptotic cells by flow cytometry. *Methods Cell Sci* 2003;25:185–94.
- [40] Amonkar SV, Reeves EL. Mosquito control with active principle of garlic, *Allium sativum*. *J Econ Entomol* 1970;63:1172–5.
- [41] Powis G. Anticancer drugs acting against signaling pathways. *Curr Opin Oncol* 1995;7:554–9.
- [42] Sies H. Glutathione and its role in cellular functions. *Free Radic Biol Med* 1999;27:16–21.
- [43] Moran LK, Gutteridge JM, Quinlan GJ. Thiols in cellular redox signalling and control. *Curr Med Chem* 2001;8:763–72.
- [44] Meister A. Glutathione metabolism. *Methods Enzymol* 1995;251:3–7.
- [45] Lash LH. Mitochondrial glutathione transport: physiological, pathological and toxicological implications. *Chem Biol Interact* 2006;163:54–67.
- [46] Jewell SA, Bellomo G, Thor H, Orrenius S, Smith M. Bleb formation in hepatocytes during drug metabolism is caused by disturbances in thiol and calcium ion homeostasis. *Science* 1982;217:1257–9.
- [47] Meister A. Mitochondrial changes associated with glutathione deficiency. *Biochim Biophys Acta* 1995;1271:35–42.
- [48] Kuriyama R, Sakai H. Role of tubulin-SH groups in polymerization to microtubules. Functional-SH groups in tubulin for polymerization. *J Biochem (Tokyo)* 1974;76:651–4.
- [49] Li M, Ciu JR, Ye Y, Min JM, Zhang LH, Wang K, et al. Antitumor activity of Z-ajoene, a natural compound purified from garlic: antimetabolic and microtubule-interaction properties. *Carcinogenesis* 2002;23:573–9.
- [50] Xiao D, Pinto JT, Soh JW, Deguchi A, Gundersen GG, Palazzo AF, et al. Induction of apoptosis by the garlic-derived compound S-allylmercaptocysteine (SAMC) is associated with microtubule depolymerization and c-Jun NH(2)-terminal kinase 1 activation. *Cancer Res* 2003;63:6825–37.
- [51] Nishida E, Kobayashi T. Relationship between tubulin SH groups and bound guanine nucleotides. *J Biochem (Tokyo)* 1977;81:343–7.
- [52] Thornberry NA. Caspases: key mediators of apoptosis. *Chem Biol* 1998;5:R97–R103.
- [53] Patya M, Zahalka MA, Vanichkin A, Rabinkov A, Miron T, Mirelman D, et al. Allicin stimulates lymphocytes and elicits an antitumor effect: a possible role of p21(ras). *Int Immunol* 2004;16:275–81.
- [54] Filomeni G, Aquilano K, Rotilio G, Ciriolo MR. Antiapoptotic response to induced GSH depletion: involvement of heat shock proteins and NF-kappaB activation. *Antioxid Redox Signal* 2005;7:446–55.
- [55] McStay GP, Clarke SJ, Halestrap AP. Role of critical thiol groups on the matrix surface of the adenine nucleotide translocase in the mechanism of the mitochondrial permeability transition pore. *Biochem J* 2002;367:548.

A novel molecule 'shati' increases dopamine uptake via the induction of tumor necrosis factor- α in pheochromocytoma-12 cells

Minae Niwa,*†‡ Atsumi Nitta,† Xiaobo Cen,† Kiyoyuki Kitaichi,§ Norio Ozaki,* Kiyofumi Yamada† and Toshitaka Nabeshima†‡

*Department of Psychiatry, Nagoya University Graduate School of Medicine, Nagoya, Japan

†Department of Neuropsychopharmacology and Hospital Pharmacy, Nagoya University Graduate School of Medicine, Nagoya, Japan

‡Department of Chemical Pharmacology, Graduate School of Pharmaceutical Sciences, Meijo University, Nagoya, Japan

§Department of Pharmacology, Faculty of Pharmaceutical Sciences, Nagasaki International University, Nagasaki, Japan

Abstract

The psychostimulant properties of methamphetamine (METH) are associated with an increase in extracellular dopamine (DA) levels in the brain, via facilitation of DA's release from pre-synaptic nerve terminals and inhibition of its reuptake through DA transporter. Recently, we have demonstrated that tumor necrosis factor- α (TNF- α) increases DA uptake and inhibits METH dependence. Moreover, we have clarified 'shati' identified in the nucleus accumbens of mice treated with METH is involved in METH dependence. In the present study, we investigated the effects of TNF- α on DA uptake in PC12 cells and established a PC12 cell line transfected with a vector containing shati cDNA to examine the precise mechanism behind the role of shati in DA uptake. Moreover, we examined

the relationship between shati and TNF- α . TNF- α increased DA uptake via the mitogen-activated protein kinase pathway and inhibited the METH-induced decrease in DA uptake in PC12 cells. Transfection of the vector containing shati cDNA into PC12 cells, induced the expression of shati and TNF- α mRNA, accelerated DA uptake, and inhibited the METH-induced decrease in DA uptake. These results suggest that the functional roles of shati in METH-regulated behavioral changes are mediated through inhibition of the METH-induced decrease in DA uptake via TNF- α .

Keywords: addiction, dopamine (DA) uptake, methamphetamine, shati, tumor necrosis factor- α (TNF- α).
J. Neurochem. (2008) **107**, 1697–1708.

The abuse of methamphetamine (METH) has significant psychiatric and medical consequences, including dependence, psychosis, overdose, and even death (Rawson *et al.* 2002). Drugs of abuse, including METH, modulate the activity of mesolimbic dopaminergic neurons, projecting from the ventral tegmental area to the nucleus accumbens

D2-R, dopamine D2 receptor; DA, dopamine; DAT, dopamine transporter; DV, dorsoventral; ERK1/2, extracellular signal-regulated kinase 1/2; FBS, fetal bovine serum; GABA, γ -aminobutyric acid; GBR 12909, [1-(2-[bis(4-fluorophenyl)-methoxy]ethyl)-4-(3-phenylpropyl)piperazine] bimesylate hydrate; GFP, green fluorescent protein; GNAT, GCN5-related N-acetyltransferase; JNK, c-Jun N-terminal kinase; MAO, monoamine oxidase; MAP, mitogen-activated protein; MEK, mitogen-activated protein kinase kinase; METH, methamphetamine; ML, mediotlateral; NAC, nucleus accumbens; NF- κ B, nuclear factor- κ B; p38, p38 mitogen-activated protein kinase; PC12, pheochromocytoma-12; PCR, polymerase chain reaction; PD98059, 2-(2-amino-3-methoxyphenyl)-4H-1-benzopyran-4-one; RIP, serine and threonine protein kinase receptor-interacting protein; RT-PCR, reverse transcription-polymerase chain reaction; shati-AS, shati antisense oligonucleotide; shati-SC, shati-scrambled oligonucleotide; SLC6, solute carrier 6; TH, tyrosine hydroxylase; TNFR1, tumor necrosis factor type I receptor; TNF- α , tumor necrosis factor- α ; TRAF2, TNF receptor-associated factor 2; VMAT-2, vesicular monoamine transporter; VTA, ventral tegmental area.

Received August 17, 2008; revised manuscript received October 6, 2008; accepted October 8, 2008.

Address correspondence and reprint requests to Toshitaka Nabeshima, PhD, Department of Chemical Pharmacology, Meijo University Graduate School of Pharmaceutical Sciences, 150 Yagotayama, Tenpaku-ku, Nagoya 468-8503, Japan. E-mail: tnabeshi@ccmfs.meijo-u.ac.jp

Abbreviations used: AMPH, amphetamine; ANOVA, analysis of variance; AP, anteroposterior; cDNA, complementary DNA; CNS, central nervous system; CSF, cerebrospinal fluid; D1-R, dopamine D1 receptor;

(NAc) (Koob 1992; Wise 1996; Koob *et al.* 1998). The principal target for the action of METH is believed to be the dopamine transporter (DAT), which is a member of the solute carrier 6 (SLC6) gene family of Na⁺/Cl⁻ coupled transporters that also includes the neurotransmitter transporters of norepinephrine, serotonin, glycine, and γ -aminobutyric acid (GABA) (Amara and Kuhar 1993; Torres *et al.* 2003; Chen *et al.* 2004). The DAT controls dopaminergic signaling by the rapid reuptake of dopamine (DA) from synaptic clefts. As a substrate, METH not only competitively inhibits DA uptake and thereby increases synaptic DA but also promotes the reverse transport of nonvesicular DA, resulting in an efflux of DA via the DAT (Sulzer *et al.* 2005; Fog *et al.* 2006). This efflux results in a dramatic increase in extracellular DA and is believed to be of major importance for the psychostimulant properties of METH (Sulzer *et al.* 2005; Fog *et al.* 2006). However, the exact neuronal circuits and molecular cascade essential for drug dependence are still poorly understood. Moreover, the molecules related to the METH-induced increase in DA efflux are unclear.

Tumor necrosis factor- α (TNF- α) plays an important role in a variety of infectious, inflammatory, and autoimmune conditions (Vassalli 1992). TNF- α also affects the CNS directly or indirectly through the stimulation of vagal afferents (Maier and Watkins 1998). Thus, this proinflammatory cytokine is emerging as a modulator of CNS function. Recently, we have demonstrated that TNF- α activates synaptosomal and vesicular DA uptake (Nakajima *et al.* 2004). Moreover, we have reported that TNF- α and its inducer diminish METH and morphine-induced behavioral sensitization and rewarding effects by promoting plasmalemmal and vesicular DA uptake as well as attenuating the METH and morphine-induced increase in overflow of DA in the NAc (Nakajima *et al.* 2004; Niwa *et al.* 2007b,d; Niwa *et al.* 2008). TNF- α modulates cellular responses through the extracellular signal-regulated kinase 1/2 (ERK1/2) and nuclear factor- κ B (NF- κ B) signaling pathways (van Vliet *et al.* 2005). ERK1/2 regulates the surface expression and capacity of DAT (Morón *et al.* 2003). However, the mechanisms by which TNF- α regulates the uptake of DA are poorly understood.

Recently, we have identified a novel molecule 'shati' in the NAc of mice treated with METH repeatedly using the polymerase chain reaction (PCR)-select complementary DNA (cDNA) subtraction method, which is a differential and epochal cloning technique. Further, we have demonstrated that shati, which contains the sequence of GCN5-related *N*-acetyltransferase (GNAT), acetyl-CoA-binding sites, and ATP-binding sites, is involved in METH-induced hyperlocomotion, sensitization, and conditioned place preference (Niwa *et al.* 2007a). Blockage of shati expression by shati antisense oligonucleotide (shati-AS) potentiates not only the increase in extracellular DA levels, but also the

decrease in synaptosomal and vesicular DA uptake in the NAc induced by repeated METH treatment, resulting in potentiation of the METH-induced dependence (Niwa *et al.* 2007a).

Pheochromocytoma-12 (PC12) cells are useful as a model of the neuronal system and have DATs. In the present study, we investigated the effects of TNF- α on DA uptake in PC12 cells and the involvement of the mitogen-activated protein kinase kinase (MEK) pathway in the effects of TNF- α on DA uptake. Moreover, we succeeded in the transfection of a vector containing shati cDNA into PC12 cells, investigated the involvement of shati in DA uptake and the METH-induced decrease in DA uptake, and examined the relationship between shati and TNF- α by using these PC12 cells.

Materials and methods

Cell culture and transfection

PC12 cells purchased from the Riken cell bank (No. RCB0009) were cultured on poly-ornithine-coated coverslips in Dulbecco's modified Eagle's medium (Sigma-Aldrich St Louis, MO, USA) supplemented with 10% heat inactivated horse serum and 5% fetal bovine serum (Loder and Melikian 2003). We made the vector containing shati cDNA with the suggested sequence of NM_001001985 using the plasmid pcDNA-DEST53 (Invitrogen, Carlsbad, CA, USA) as an expression vector with green fluorescent protein (GFP), although N-terminal of seven amino acids of shati was missing (CDS 882-1760) in this vector. For transient expression, the cells were transfected with the plasmid expressing shati using Lipofectamine 2000 (Invitrogen).

[³H] DA uptake in PC12 cells

The uptake of [³H] DA in PC12 cells was performed as described before (Melikian and Buckley 1999). The cells were washed in Krebs-Ringers-4-(2-hydroxyethyl)-1-piperazineethanesulfonic acid buffer twice before the assay. Uptake was initiated by adding 1 μ M [³H] DA (Perkin Elmer, Waltham, MA, USA) containing 10⁻⁵ M pargyline and 10⁻³ M ascorbic acid. Uptake proceeded for 10 min at 23°C and was terminated with three rapid washes in ice-cold Krebs-Ringers-4-(2-hydroxyethyl)-1-piperazineethanesulfonic acid buffer. The amount of [³H] DA accumulated was determined by liquid scintillation counting (Beckman Coulter, Inc., Fullerton, CA, USA). Non-specific uptake was defined in the presence of 10 μ M [1-(2-bis(4-fluorophenyl)-methoxy)ethyl]-4-(3-phenylpropyl)piperazine] bimesylate hydrate (GBR 12909). The cells were pre-treated with TNF- α (0.1, 1, and 10 ng/mL) for 40 min, and assayed for [³H] DA uptake. To neutralize TNF- α in PC12 cells, the cells were pre-treated with polyclonal goat anti-TNF- α antibody (R&D Systems Ltd., Minneapolis, MN, USA; Ab; 1, 10, 50, and 100 ng/mL) or soluble TNF receptor I (R&D Systems Ltd, sRI; 0.1, 0.5, 1, and 10 ng/mL) 10 min before the treatment with TNF- α (10 ng/mL, 40 min) (Barone *et al.* 1997), and assayed for [³H] DA uptake. The function of TNF- α is mediated through two distinct cell surface receptors, TNF receptor I and TNF receptor II. The majority of TNF functions are mediated primarily through TNF receptor I, whereas TNF receptor II seems to play a role in only a limited number of

TNF responses (Hsu *et al.* 1995). Moreover, it has been reported that immunoreactivity for TNF receptor I is found in cell bodies and process of dopaminergic neurons (Boka *et al.* 1994). Therefore, we have used soluble TNF receptor I for neutralization for TNF- α . To examine the involvement of the MEK pathway in the TNF- α -induced increase in DA uptake in PC12 cells, the cells were pre-treated with a selective MEK inhibitor 2-(2-amino-3-methoxyphenyl)-4H-1-benzopyran-4-one (Calbiochem, San Diego, CA, USA; PD98059; 1, 10, 100, and 500 μ M) 10 min before their treatment with TNF- α (10 ng/mL, 40 min), and assayed for [3 H] DA uptake. PD98059 was dissolved in dimethyl sulfoxide to give a concentration of 50 mM, stored in aliquots at -80°C , and diluted in Dulbecco's modified Eagle's medium to 1–500 μ M immediately prior to use. To examine the effects of TNF- α on the METH-induced decrease in DA uptake in PC12 cells, the cells were pre-treated with TNF- α (10 ng/mL) 10 min before being treated with METH (1 μ M, 30 min), and assayed for [3 H] DA uptake, following previous observations (Nakajima *et al.* 2004). Cen *et al.* (2008) have reported that METH (1 μ M) decreases plasmalemmal DAT expression in time-dependent manner (0, 5, 15, 30, 60 min), which is paralleled with the decrease in [3 H] DA uptake. Since treatment of METH (1 μ M) for 30 min significantly decreases DA uptake compared with control group (Cen *et al.*, 2008), we have selected this time point for treatment of METH before the uptake assay. To examine the involvement of TNF- α in the shati-induced increase in [3 H] DA uptake in the shati-over-expressing PC12 cells, the cells were pre-treated with polyclonal goat anti-TNF- α antibody (R&D Systems Ltd, Ab; 50 ng/mL) or soluble TNF receptor I (R&D Systems Ltd, sR I; 1 ng/mL) 10 min before their treatment with METH (1 μ M, 30 min), and assayed for [3 H] DA uptake.

Immunocytochemistry

Two antibodies against the peptide of the hypothetical protein, CNTAFRGLRQHPRTQLL (S-3) and CMSVDSFRGKGIKALG (S-4) unique to shati were generated. These peptides were conjugated to keyhole limpet hemocyanin and injected into rabbits six times at 1-week intervals. Serum was taken from the rabbits 1 week after the final injection. The serum was diluted 200 times for immunostaining (Niwa *et al.* 2007a).

Transfected PC12 cells attached to glass coverslips were fixed with 4% paraformaldehyde in phosphate-buffered saline for 20 min, and then blocked in 3% normal sera and 0.1% Triton X-100 for 1 h. The coverslips were incubated with primary antibodies at 4°C overnight, washed with phosphate-buffered saline, and then incubated with appropriate secondary antibodies for 2 h. Polyclonal rabbit anti-S-3 or anti-S-4 antibody (1 : 200), monoclonal mouse anti-tyrosine hydroxylase (TH) antibody (1 : 200, Chemicon, Temecula, CA, USA), monoclonal mouse anti-GFP antibody (1 : 500, Chemicon), polyclonal goat anti-rat TNF- α antibody (1 : 100, R&D Systems Ltd), and polyclonal rabbit anti-GFP antibody (1 : 100, Chemicon) served as primary antibodies. Goat anti-mouse Alexa Fluor 546 (1 : 1000, Invitrogen), donkey anti-goat Alexa Fluor 546 (1 : 1000, Invitrogen), rabbit anti-mouse Alexa Fluor 488 (1 : 1000, Invitrogen), and donkey anti-rabbit Alexa Fluor 488 (1 : 1000, Invitrogen) were used as secondary antibodies. After being washed and mounted, stained cells were observed under a fluorescence microscope (Axioskop 2 plus). Because similar results were obtained using

the anti S-3 and anti-S-4 antibodies in the immunohistochemical experiments, only the data obtained with the anti-S-4 antibody is described.

Real time reverse transcription-polymerase chain reaction

Total RNA was isolated using an RNeasy Kit (Qiagen, Hilden, Germany) and converted into cDNA using a SuperScriptTM First-Strand System for RT-PCR Kit (Invitrogen). The levels of shati and TNF- α mRNA were determined by real-time RT-PCR using a TaqMan probe. The 18S ribosomal RNA was used as the internal control (Applied Biosystems, CA, USA). The shati primers used for real-time RT-PCR were as follows: 5'-TGTAACACCCCTAAAGTGCCCT-3' (forward; bp 2967–2989) and 5'-TCAATCCTGCATACAAGGAATCAA-3' (reverse; bp 3022–3045), and the TaqMan probe was 5'-CACAGTCTGTGAGGCTCAGGTTGCC-3' (probe; bp 2995–3020). The amplification consisted of an initial step (95°C for 5 min) and then 40 cycles of denaturation for 30 sec at 95°C , annealing for 40 s at 59°C , and the extension time for 1 min at 72°C in an iCycle iQ Detection System (Bio-Rad Laboratories, Inc., CA, USA) (Niwa *et al.* 2007a). The expression levels were calculated as described previously (Wada *et al.* 2000).

Animals

The male C57BL/6J- wild-type mice were obtained from Slc Japan (Hamamatsu, Japan). Animals were housed in plastic cages and kept in a temperature-, humidity-, and light-controlled room ($23 \pm 1^{\circ}\text{C}$; $50 \pm 5\%$ humidity; 12 : 12 h light/dark cycle starting at 8:00 AM) and had free access to food and water, except during behavioral experiments. All animal care and use was in accordance with the National Institutes of Health Guide for the Care and Use of Laboratory Animals and approved by the Institutional Animal Care and Use Committee of Nagoya University School of Medicine. Animals were treated according to the Guidelines of Experimental Animal Care issued from the Japanese Pharmaceutical Society.

Shati-antisense oligonucleotide (shati-AS) treatment

Mice were anesthetized with pentobarbital (40 mg/kg, i.p.) and placed in a stereotaxic apparatus. The infusion cannula was connected to a miniosmotic pump (total capacity was 90 μ L, Alzet 1002; Alza, Palo Alto, CA, USA) filled with shati-antisense oligonucleotide (shati-AS) or -scrambled oligonucleotide (shati-SC). The pump was implanted into the right ventricle [anteroposterior (AP) -0.5 mm, mediolateral $+1.0$ mm from the bregma, and dorsoventral -2.0 mm from the skull, according to the atlas of Franklin and Paxinos (1997)]. Phosphorothionate oligonucleotides were custom-synthesized at Nissinbo Biotechnology (Tokyo, Japan) and dissolved in artificial CSF (147 mM NaCl, 3 mM KCl, 1.2 mM CaCl₂, and 1.0 mM MgCl₂, pH 7.2). The oligonucleotides were phosphorothioated at the first three bases of both the 5'- and 3'-ends, which results in increased stability and less toxicity. The sequences of shati-AS and -SC were 5'-TCTTCGTCGCAGACATGTGCG-3' and 5'-GGTCTGCTACTGCTGCTAGTC-3', respectively. Shati-AS and -SC were continuously infused into the cerebral ventricle at a dose of 1.8 nmol/6 μ L/day (flow rate, 0.25 μ L/h). Additionally, shati-SC was used as a control. Three days after the start of oligonucleotide infusion, mice were

administered METH (1 mg/kg, s.c.) for 5 days and decapitated 2 h after the final treatment (Niwa *et al.* 2007a).

Statistical analysis

All data were expressed as means \pm SE. Statistical differences between two groups were determined with Student's *t*-test. Statistical differences among three groups or more were determined using a one-way analysis of variance (ANOVA), two-way ANOVA, or three-way ANOVA, followed by the Bonferroni multiple comparison test. $p < 0.05$ was regarded as statistically significant.

Nucleotide sequences

The DNA Data Bank of Japan/GenBank/European Molecular Biology Laboratory accession number for the primary nucleotide sequence of shati is DQ174094.

Results

Effect of TNF- α on DA uptake in PC12 cells

First, we investigated the effects of TNF on DA uptake in PC12 cells, since we have recently demonstrated that TNF- α activates synaptosomal and vesicular DA uptake in mice (Nakajima *et al.* 2004).

TNF- α (10 ng/mL, 40 min) increased [3 H] DA uptake compared with the control group ($F_{3,28} = 4.933$, $p < 0.01$, one-way ANOVA) (Fig. 1a). Moreover, we investigated whether the TNF- α -induced increase was antagonized by the anti-TNF- α antibody and soluble TNF receptor in PC12 cells. Pre-treatment with the antibody (10, 50, and 100 ng/

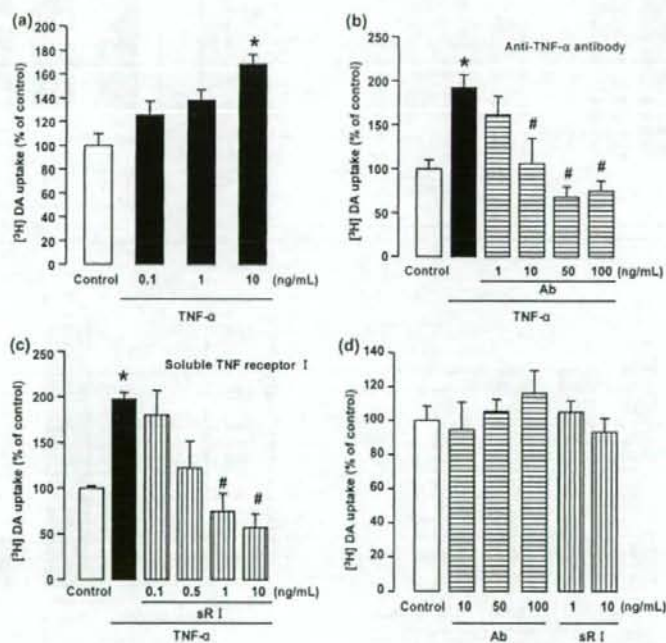


Fig. 1 Effects of anti-TNF- α antibody (Ab) or soluble TNF receptor I (sR I) on TNF- α -induced increase in [3 H] DA uptake in PC12 cells. (a) The cells were pre-treated with TNF- α (0.1, 1, and 10 ng/mL) for 40 min, and assayed for [3 H] DA uptake. The [3 H] DA uptake was 0.14 ± 0.01 pmol/10 min for control. The final concentration of [3 H] DA was 20 nM. Values are means \pm SE ($n = 8$). * $p < 0.05$ versus control. (b) Effects of anti-TNF- α antibody (Ab) on TNF- α -induced increase in [3 H] DA uptake in PC12 cells. The cells were pre-treated with anti-TNF- α antibody (1, 10, 50, and 100 ng/mL) 10 min before their treatment with TNF- α (10 ng/mL, 40 min), and assayed for [3 H] DA uptake. The [3 H] DA uptake was 0.10 ± 0.02 pmol/10 min for the control. The final concentration of [3 H] DA was 20 nM. Values are means \pm SE ($n = 6-7$). * $p < 0.05$ versus control. # $p < 0.05$ versus TNF- α -treated cells. (c) Effects of soluble TNF receptor I (sR I) on TNF- α -induced

increase in [3 H] DA uptake in PC12 cells. The cells were pre-treated with soluble TNF receptor I (0.1, 0.5, 1, and 10 ng/mL) 10 min before being treated with TNF- α (10 ng/mL, 40 min), and assayed for [3 H] DA uptake. The [3 H] DA uptake was 0.06 ± 0.00 pmol/10 min for the control. The final concentration of [3 H] DA was 20 nM. Values are means \pm SE ($n = 6-7$). * $p < 0.05$ versus control. # $p < 0.05$ versus TNF- α -treated cells. (d) Effects of anti-TNF- α antibody (Ab) or soluble TNF receptor I (sR I) on [3 H] DA uptake in PC12 cells. The cells were pre-treated with anti-TNF- α antibody (10, 50, and 100 ng/mL) or soluble TNF receptor I (1 and 10 ng/mL) for 50 min, and assayed for [3 H] DA uptake. The [3 H] DA uptake was 0.08 ± 0.01 pmol/10 min for the control. The final concentration of [3 H] DA was 20 nM. Values are means \pm SE ($n = 6-8$).

mL, 50 min) or soluble TNF receptor I (1 and 10 ng/mL, 50 min) significantly inhibited the TNF- α -induced increase in [3 H] DA uptake ($F_{5,34} = 7.370$ for anti-TNF- α antibody; $F_{5,34} = 7.526$ for soluble TNF receptor I, $p < 0.01$, one-way ANOVA) (Fig. 1b and c), although the anti-TNF- α antibody (10, 50, and 100 ng/mL, 50 min) or soluble TNF receptor I (1 and 10 ng/mL, 50 min) itself had no effect on DA uptake (Fig. 1d). These results suggest that TNF- α activates DA uptake in PC12 cells.

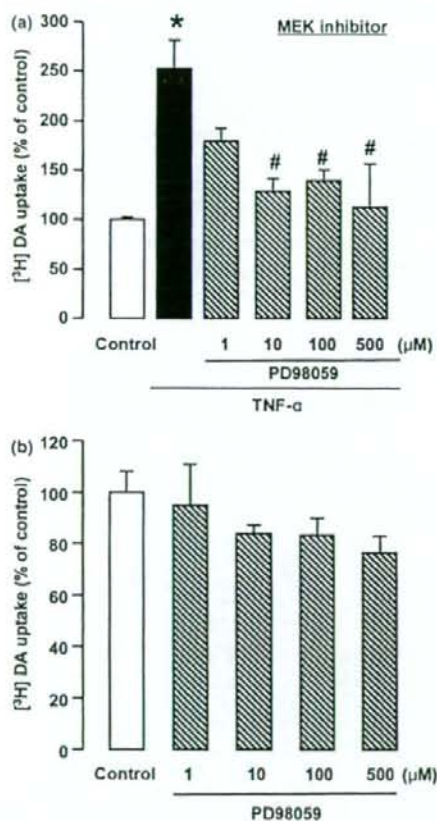


Fig. 2 Effects of MEK inhibitor on TNF- α -induced increase in [3 H] DA uptake in PC12 cells. (a) Effects of the MEK inhibitor PD98059 on TNF- α -induced increase in [3 H] DA uptake in PC12 cells. The cells were pre-treated with PD98059 (1, 10, 100, and 500 μ M) 10 min before their treatment with TNF- α (10 ng/mL, 40 min), and assayed for [3 H] DA uptake. The [3 H] DA uptake was 0.10 ± 0.00 pmol/10 min for control. The final concentration of [3 H] DA was 20 nM. Values are means \pm SE ($n = 4$). * $p < 0.05$ versus control, # $p < 0.05$ versus TNF- α -treated cells. (b) Effects of PD98059 on [3 H] DA uptake in PC12 cells. The cells were pre-treated with PD98059 (1, 10, 100, and 500 μ M) for 50 min, and assayed for [3 H] DA uptake. The [3 H] DA uptake was 0.12 ± 0.00 pmol/10 min for the control. The final concentration of [3 H] DA was 20 nM. Values are means \pm SE ($n = 4$).

Effects of mitogen-activated protein kinase inhibitor on TNF- α -induced increase in DA uptake in PC12 cells

TNF- α modulates cellular responses through the ERK1/2 signaling pathway (van Vliet *et al.* 2005). Therefore, we investigated whether the TNF- α -induced increase in DA

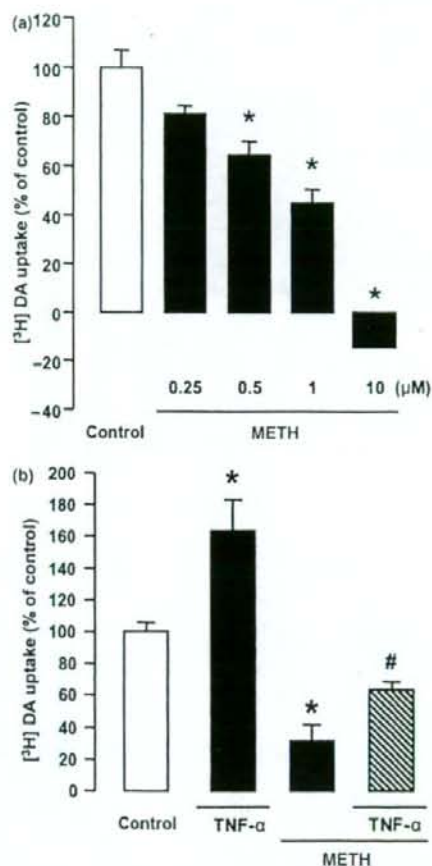


Fig. 3 Effects of TNF- α on METH-induced decrease in [3 H] DA uptake in PC12 cells. (a) Dose-response effects of METH on [3 H] DA uptake in PC12 cells. The cells were pre-treated with METH (0.25, 0.5, 1, and 10 μ M) for 30 min, and assayed for [3 H] DA uptake. The [3 H] DA uptake was 0.28 ± 0.02 pmol/10 min for the control. The final concentration of [3 H] DA was 20 nM. Values are means \pm SE ($n = 4$). * $p < 0.05$ versus control. (b) Effects of TNF- α on METH-induced decrease in [3 H] DA uptake in PC12 cells. The cells were pre-treated with TNF- α (10 ng/mL) 10 min before being treated with METH (1 μ M, 30 min), and assayed for [3 H] DA uptake. The [3 H] DA uptake was 0.19 ± 0.01 pmol/10 min for the control. The final concentration of [3 H] DA was 20 nM. Values are means \pm SE ($n = 5$). * $p < 0.05$ versus control, # $p < 0.05$ versus METH-treated cells.

uptake was antagonized by the MEK inhibitor PD98059 in PC12 cells.

Pre-treatment with PD98059 (10, 100, and 500 μ M, 50 min) significantly inhibited the TNF- α -induced increase in [3 H] DA uptake ($F_{5,18} = 5.961$, $p < 0.01$, one-way ANOVA) (Fig. 2a), although PD98059 (1, 10, 100, and 500 μ M, 50 min) itself had no effect on the uptake (Fig. 2b). These results suggest that TNF- α activates DA uptake via the MEK signaling pathway in PC12 cells.

Effects of TNF- α on METH-induced decrease in DA uptake in PC12 cells

We have previously demonstrated that TNF- α and its inducer diminish the METH-induced decrease in DA uptake and inhibit the rewarding effects of and sensitization to METH (Nakajima *et al.* 2004; Niwa *et al.* 2007c, e). Therefore, we confirmed the effects of TNF- α on the METH-induced decrease in DA uptake in PC12 cells.

METH (0.5, 1, and 10 μ M, 30 min) decreased [3 H] DA uptake compared with the control group in a dose-dependent manner ($F_{4,15} = 83.675$, $p < 0.01$, one-way ANOVA) (Fig. 3a). Moreover, TNF- α (10 ng/mL, 40 min) inhibited the METH-induced decrease in [3 H] DA uptake (TNF- α , $F_{1,16} = 14.759$, $p < 0.01$; METH, $F_{1,16} = 45.994$, $p < 0.01$; TNF- α -METH $F_{1,16} = 1.573$, $p = 0.228$; two-way ANOVA) (Fig. 3b). These results suggest that TNF- α inhibits the METH-induced decrease in DA uptake in PC12 cells (Fig. 3) as well as promoting plasmalemmal and vesicular DA uptake

to diminish METH and morphine-induced behavioral sensitization and rewarding effects (Nakajima *et al.* 2004; Niwa *et al.* 2007b; Niwa *et al.* 2008).

Transfection of the vector containing shati cDNA into PC12 cells

We established a PC12 cell line transfected with the vector containing shati cDNA to examine the role of shati in DA uptake and the METH-induced decrease in DA uptake.

We used immunostaining for TH to check morphological changes of the PC12 cells after the transfection of the vector containing shati cDNA. Morphological changes to the cells were not observed after the transfection compared with mock-transfected or non-transfected PC12 cells (Fig. 4a). To confirm the transfection of the vector containing shati cDNA, we checked for immunostaining against S-4 and GFP, co-expressed with shati. No immunoreactivity for S-4 or GFP was found in the cells that were mock-transfected, which express neither shati nor GFP [Fig. 4b (i)]. The cells mock-transfected (=expression vector [pcDNA-DEST53]), which express GFP, but not shati, were immunopositive for GFP, but not S-4 [Fig. 4b (ii)]. The cells transfected with the vector containing shati cDNA, which express both shati and GFP, were immunopositive for S-4 and GFP [Fig. 4b (iii)]. The cells immunopositive for S-4 were merged with those positive for GFP. These results indicated that shati was certainly expressed in PC12 cells and transfection did not affect cell survival or morphology.

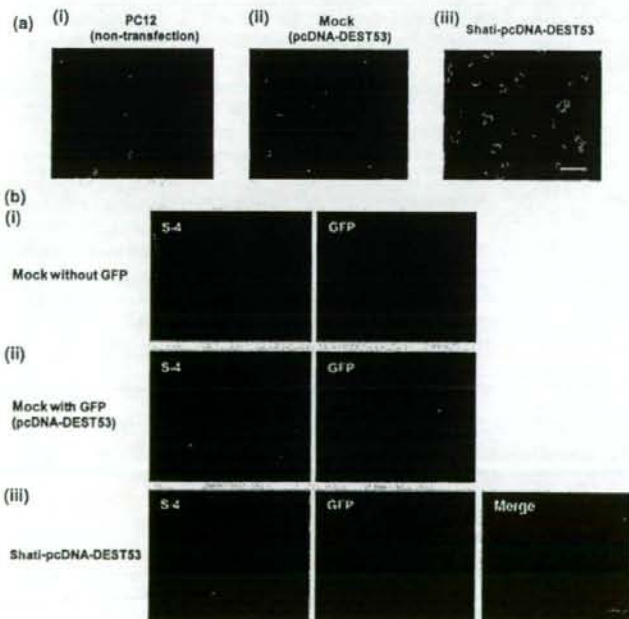


Fig. 4 Transfection of the vector containing shati cDNA into PC12 cells. (a) The morphological changes of the PC12 cells after transfection of the expression vector (pcDNA-DEST53) (ii) or vector containing shati cDNA (iii). The expression vector alone (mock-transfection) (ii), or the vector containing shati cDNA (iii) was introduced into PC12 cells. There were no changes in survival or morphology in the transfected PC12 cells. Scale bar: 20 μ m. (b) Immunostaining of shati in PC12 cells transfected with the vector containing shati cDNA. pENTR/TEV/D-TOPO (without shati recombination and green fluorescent protein (GFP) site) (i), pcDNA-DEST53 with GFP (mock-transfection) (ii), or the vector containing shati cDNA and GFP (iii), was introduced into PC12 cells. The shati-immunopositive cells (green) were colocalized with GFP-immunopositive cells (red). Double immunostaining for S-4 and GFP in PC12 cells transfected with the vector containing shati cDNA reveals overexpression of shati in PC12 cells (iii). Scale bar: 20 μ m.

Effect of over-expressed shati on DA uptake in PC12 cells
We have previously demonstrated that shati-AS, which inhibits the expression of shati mRNA, significantly potentiates the METH-induced decrease in synaptosomal and vesicular [3 H] DA uptake compared with that in the shati-SC or CSF-treated mice (Niwa *et al.* 2007a). Moreover, [3 H] DA uptake in saline-treated mice was also decreased by shati-AS compared with that in the CSF-treated mice, although shati-SC had no effect on [3 H] DA uptake (Niwa *et al.* 2007a). Given the results for synaptosomal and vesicular [3 H] DA uptake using shati-AS, we concluded that shati plays a critical role in modulating DA uptake. To address this issue, we investigated the role of shati in DA uptake in PC12 cells transfected with the vector containing shati cDNA.

Transfection of the vector containing shati cDNA increased shati mRNA expression compared with the mock-transfection, suggesting that shati was over-expressed in these cells (Fig. 5a left two columns). The increase in the levels of shati mRNA expression evoked by METH treatment (1 μ M, 30 min) in mock-transfected cells was significantly potentiated by shati over-expression in PC12 cells (drug, $F_{1,28} = 20.917$, $p < 0.01$; transfection, $F_{1,28} = 247.684$, $p < 0.01$; drug \times transfection, $F_{1,28} = 0.003$, $p = 0.955$; two-way ANOVA) (Fig. 5a right two columns).

We examined the *in vitro* effect of over-expressed shati on [3 H] DA uptake in PC12 cells. Shati-over-expressing cells themselves showed increased [3 H] DA uptake compared with the mock-transfected cells, suggesting that shati itself promotes DA uptake (Fig. 5b left two columns). We pre-treated PC12 cells with METH (1 μ M) for 30 min, and then assayed the uptake of [3 H] DA. As shown in Fig. 5b, METH (1 μ M, 30 min) decreased [3 H] DA uptake compared with the mock-transfected control cells. In the shati-over-expressing cells, the METH-induced decrease in [3 H] DA uptake was significantly inhibited compared with that in the mock-transfected cells (drug, $F_{1,40} = 45.807$, $p < 0.01$; transfection, $F_{1,28} = 21.551$, $p < 0.01$; drug \times transfection, $F_{1,28} = 0.001$, $p = 0.971$; two-way ANOVA) (Fig. 5b right two columns). These results indicated that shati could attenuate METH-induced inhibition of DA uptake.

Regulation of TNF- α expression by shati

TNF- α activates synaptosomal and vesicular DA uptake (Nakajima *et al.* 2004). TNF- α and its inducer diminish the METH-induced decrease in DA uptake and inhibit the METH-induced dependence (Nakajima *et al.* 2004; Niwa *et al.* 2007c, e). Moreover, given the findings on [3 H] DA uptake obtained using shati-AS (Niwa *et al.* 2007a) and shati-over-expressing cells (Fig. 5b), we hypothesized that shati increased DA uptake by regulating TNF- α . To address this issue, we examined expression levels of TNF- α mRNA after transfection of the vector containing shati cDNA or treatment with shati-AS.

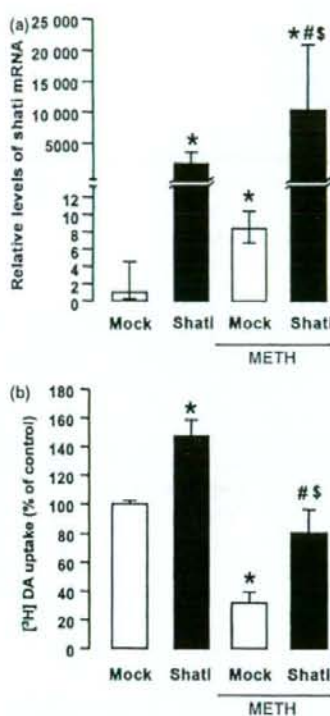


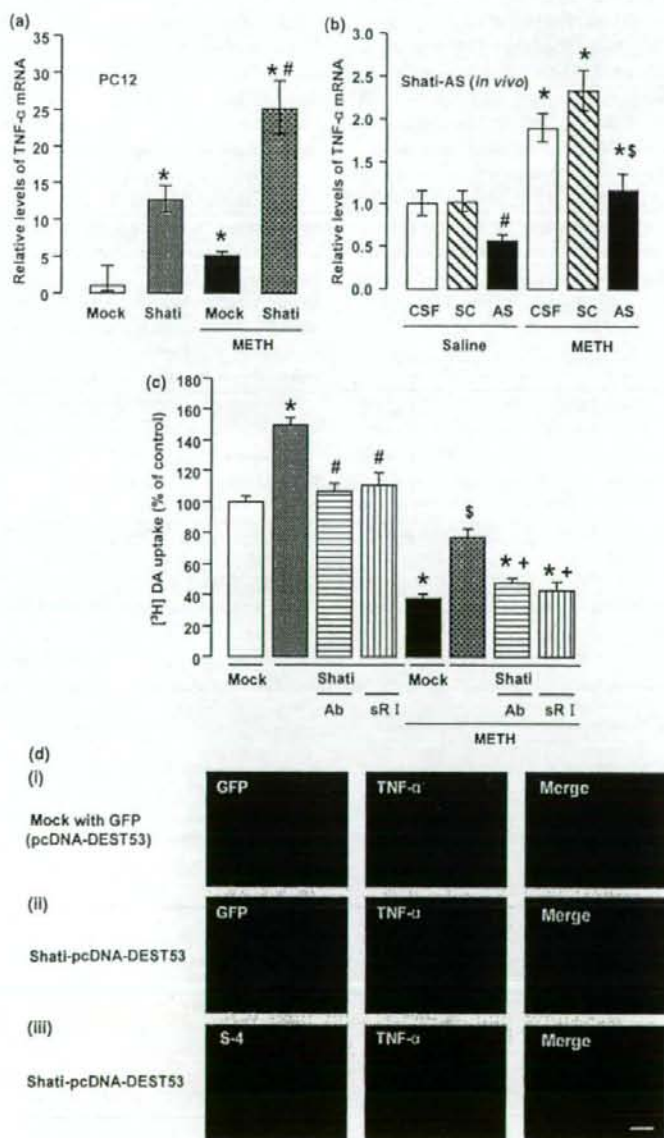
Fig. 5 Effect of overexpression of shati on DA uptake in PC12 cells. (a) Shati mRNA expression in PC12 cells transfected with the vector containing shati cDNA. The mock construct (pcDNA-DEST53), or the vector containing shati cDNA was introduced into PC12 cells. These cells were treated with 1 μ M METH for 30 min. Values are means \pm SE ($n = 8$). * $p < 0.05$ versus mock-transfected cells. # $p < 0.05$ versus the vector containing shati cDNA-transfected cells. § $p < 0.05$ versus METH + mock-transfected cells. (b) Effect of overexpression of shati on [3 H] DA uptake in PC12 cells. The mock construct (pcDNA-DEST53), or the vector containing shati cDNA was introduced into PC12 cells. The cells were pre-treated with 1 μ M METH for 30 min, and [3 H] DA uptake was measured. The [3 H] DA uptake was 0.12 ± 0.02 pmol/10 min for the mock-transfected cells. The final concentration of [3 H] DA was 20 nM. Values are means \pm SE ($n = 10-12$). * $p < 0.05$ versus mock-transfected cells. # $p < 0.05$ versus the vector containing shati cDNA-transfected cells. § $p < 0.05$ versus METH + mock-transfected cells.

Shati-over-expressing cells themselves had increased TNF- α mRNA expression compared with the mock-transfected cells (Fig. 6a left two columns), suggesting that shati regulates expression of TNF- α in PC12 cells. The increase in TNF- α mRNA expression evoked by METH treatment (1 μ M, 30 min) in mock-transfected cells was significantly potentiated by overexpression of shati *in vitro* (drug, $F_{1,28} = 21.000$, $p < 0.01$; transfection, $F_{1,28} = 65.860$,

$p < 0.01$; drug \times transfection, $F_{1,28} = 3.557$, $p = 0.070$; two-way ANOVA (Fig. 6a right two columns). As shown in Fig. 6b right three columns, the increase in TNF- α mRNA expression evoked by repeated METH treatment in the NAc was significantly abolished by shati-AS, although shati-SC had no effect. Moreover, TNF- α mRNA expression in the NAc of saline-treated mice was also inhibited by shati-AS, although not by shati-SC (drug, $F_{1,47} = 48.473$, $p < 0.01$;

intracerebroventricular treatment, $F_{2,47} = 15.670$, $p < 0.01$; drug \times intracerebroventricular treatment, $F_{2,47} = 0.239$, $p = 0.788$; two-way ANOVA) (Fig. 6b left three columns), indicating that shati-AS decreases effectively the expression of TNF- α mRNA through the down-regulation of shati mRNA expression.

As shown in Fig. 6c, right four columns, the ameliorative effect of shati on the METH-induced decrease in DA uptake



was antagonized by treatment with the TNF- α antibody (50 ng/mL) or soluble TNF receptor I (1 ng/mL). The shati-induced potentiation of DA uptake was also inhibited by the treatments in shati-over-expressing cells (drug, $F_{1,72} = 296.090$, $p < 0.01$; transfection, $F_{1,72} = 13.864$, $p < 0.01$; neutralization, $F_{1,72} = 32.930$, $p < 0.01$; drug \times transfection, $F_{1,72} = 0.189$, $p = 0.665$; drug \times neutralization, $F_{1,72} = 1.496$, $p = 0.225$; transfection \times neutralization, $F_{1,72} = 34.828$, $p < 0.01$; drug \times transfection \times neutralization, $F_{1,72} = 0.003$, $p = 0.958$; three-way ANOVA) (Fig. 6c left four columns). These results suggest that over-expression of shati increased DA uptake by regulating TNF- α in PC12 cells. To confirm the relationship between shati and TNF- α , we examined immunostaining for GFP, which is co-expressed with shati, or S-4 and TNF- α . The cells mock-transfected, which express GFP, but not shati, were immunopositive for GFP, but not TNF- α . The cells transfected with the vector containing shati cDNA, which express both GFP and shati, were immunopositive for GFP or S-4 and TNF- α . The cells immunopositive for S-4 were merged with those positive for TNF- α . These results indicated that shati was expressed in TNF- α -immunopositive cells (Fig. 6d).

Discussion

DA is the predominant catecholamine neurotransmitter in the CNS. Disruptions of DA signaling contribute to various psychiatric and neurological disorders, including drug addiction, schizophrenia, and Parkinson's disease (Self and Nestler 1995; Hyman 1996). Extracellular DA levels are primarily regulated by DAT, an integral membrane protein that is a member of the Na⁺/Cl⁻-dependent co-transporter gene family (Amara and Kuhar 1993). By removing extracellular DA and recycling it back to the neuron, DAT plays an essential role in terminating DA signaling. Pharmacological blockade of DAT by psychostimulants inhibits the reuptake of DA from the extracellular space, resulting in

increased extracellular DA levels and augmented receptor stimulation (Horn 1990). Although pharmacological and genetic ablation (Grace 1995; Jones *et al.* 1998) studies indicate a critical role for DAT in the maintenance of DA neuronal homeostasis, the endogenous mechanisms regulating DAT expression and activity are poorly understood.

The PC12 cell line is derived from the rat pheochromocytoma. It is often used as an *in vitro* model to understand the physiology of central DA neurons (Roda *et al.* 1980; Tischler 2002; Fornai *et al.* 2007). A number of factors contribute to the wide use of PC12 cells: they are inexpensive as well as easy to handle, and mimic many features of central DA neurons. In fact, PC12 cells produce catecholamines (Markey *et al.* 1980; Roda *et al.* 1980; Vaccaro *et al.* 1980). In particular, they contain DA (Greene and Rein 1978) as the main catecholamine and bear DA receptors on their external membrane (Sampath *et al.* 1994). In light of the presence of DA and DA receptors, as well as DA uptake mechanisms, PC12 cell lines are considered to be closer to DA terminals than their ancestors (i.e. chromaffin cells of the adrenal medulla). This concept is reinforced by the presence of monoamine oxidase type A, which also characterizes DA neurons (Finberg and Youdim 1983), in contrast with the established prevalence of monoamine oxidase type B within chromaffin cells of the adrenal medulla (Youdim 1991).

Recently, we have demonstrated that TNF- α and its inducer play a neuroprotective role in the behavioral sensitization to and rewarding effects of METH by activating plasmalemmal and vesicular DAT as well as by inhibiting the METH-induced increase in extracellular DA levels (Nakajima *et al.* 2004; Niwa *et al.* 2007c,e). TNF- α modulates cellular responses through the ERK1/2 and NF- κ B signaling pathways (van Vliet *et al.* 2005). The adaptor protein TNF receptor-associated factor 2 (TRAF2) and the serine and threonine protein kinase receptor-interacting protein are required for optimal TNF-induced signaling through ERK1/2, c-Jun N-terminal kinase (JNK) and p38 mitogen-activated

Fig. 6 Involvement of TNF- α in shati-induced increase in DA uptake in PC12 cells. (a) TNF- α mRNA expression in PC12 cells transfected with the vector containing shati cDNA. The expression vector alone (pcDNA-DEST53), or the vector containing shati cDNA was introduced into PC12 cells. The cells were treated with 1 μ M METH for 30 min. Values are means \pm SE ($n = 8$). * $p < 0.05$ versus mock-transfected group. # $p < 0.05$ versus METH + mock-transfected group. (b) Effect of shati-AS on TNF- α mRNA expression. Mice were administered METH (1 mg/kg, s.c.) for 5 days and decapitated 2 h after the final treatment. Values are means \pm SE ($n = 8-10$). * $p < 0.05$ versus corresponding saline-treated mice. # $p < 0.05$ versus saline + CSF and saline + shati-SC-treated mice. * $p < 0.05$ versus METH + CSF and METH + shati-SC-treated mice. (c) Involvement of TNF- α in shati-induced increase in [³H] DA uptake in PC12 cells. The expression vector alone (pcDNA-DEST53), or the vector containing shati cDNA was introduced into PC12 cells. The cells were pre-treated with anti-TNF- α antibody (Ab;

50 ng/mL) or soluble TNF receptor I (sR; 1 ng/mL) 10 min before their treatment with METH (1 μ M, 30 min), and assayed for [³H] DA uptake. The [³H] DA uptake was 0.15 \pm 0.02 pmol/10 min for the mock-transfected group. The final concentration of [³H] DA was 20 nM. Values are means \pm SE ($n = 10$). * $p < 0.05$ versus mock-transfected group. # $p < 0.05$ versus the vector containing shati cDNA-transfected group. * $p < 0.05$ versus METH + mock-transfected group. * $p < 0.05$ versus METH + the vector containing shati cDNA-transfected group. (d) Immunostaining of shati and TNF- α in PC12 cells transfected with the vector containing shati cDNA. The expression vector alone (pcDNA-DEST53) (i), or the vector containing shati cDNA (ii) (iii) was introduced into PC12 cells. The GFP or shati-immunopositive cells (green) were co-localized with TNF- α -immunopositive cells (red) (ii) (iii). Double immunostaining for GFP or S-4 and TNF- α in PC12 cells transfected with the vector containing shati cDNA reveals expression of shati in TNF- α -immunopositive cells (ii) (iii). Scale bar: 20 μ m.

protein kinase (p38) (Baud and Karin 2001; Devin *et al.* 2003). MEK inhibitor PD98059 significantly decreases phosphorylated ERK1/2 without affecting total ERK level, MEK-JNK, -p38, and -NF- κ B, resulting in loss of DAT surface expression and DAT capacity. According to these results, MEK-ERK pathway, but not MEK-JNK, -p38, or -NF- κ B pathway, is important for intracellular trafficking and transport capacity of DAT (Morón *et al.* 2003). Therefore, we investigated the involvement of TNF- α in DA uptake and the METH-induced inhibition of DA uptake in PC12 cells. Moreover, we examined the involvement of MEK-ERK signaling in the effects of TNF on DA uptake. TNF- α increased DA uptake via the MEK-ERK signaling pathway in PC12 cells (Figs 1 and 2). The increase was antagonized by the anti-TNF- α antibody and soluble TNF receptor I (Fig. 1b and c), suggesting that TNF- α certainly increases DA uptake in PC12 cells. Moreover, TNF- α inhibited the METH-induced decrease in DA uptake in PC12 cells (Fig. 3b). We have previously reported that the kinetics of [3 H] DA uptake in the absence or presence of TNF- α (10 ng/mL). Lineweaver-burk plots show that TNF- α potentiates [3 H] DA uptake by increasing the affinity (K_m) accompanied by reducing the maximum number of [3 H] DATs (V_{max}) (Nakajima *et al.* 2004). We suggest that TNF- α modulates the function of DAT, although it also regulates the expression of DAT. The expression of TNF- α is induced through the activation of transcription factors such as activator protein-1 (AP-1) and NF- κ B by the activation of JNK/p38 (Guha *et al.* 2000; Rahman and MacNee 2000). Further, TNF- α acts on mitochondria to generate reactive oxygen species, which are involved in the activation of AP-1 and NF- κ B (Rahman and MacNee 2000). Changes in transcription factors may result in long-term changes in gene expression, thereby contributing to neuronal adaptations that underlie behavioral sensitization (Nestler 2001). Therefore, we hypothesized that TNF- α inhibits the METH-induced increase in extracellular DA levels in the NAc by promoting DA uptake and finally inhibits METH-induced sensitization and rewarding effects (Nakajima *et al.* 2004; Niwa *et al.* 2007c,e).

'Shati', named after the symbol for Nagoya castle, was identified among molecules whose expression was regulated in the NAc of mice treated with METH (Niwa *et al.* 2007a). Recently, we have demonstrated that blockage of shati expression by shati-AS potentiates the increase in extracellular DA levels in the NAc and the decrease in synaptosomal and vesicular DA uptake in the midbrain induced by repeated METH treatment (Niwa *et al.* 2007a). Both TNF- α and shati increase DA uptake and inhibit the METH-induced decrease in DA uptake (Nakajima *et al.* 2004; Niwa *et al.* 2007a). Therefore, we investigated the precise mechanism of the effects of shati on DA uptake, and the METH-induced inhibition of DA uptake in PC12 cells. Moreover, we examined the relationship between shati and TNF- α in PC12 cells. Over-expression of shati by transfection of the vector

containing shati cDNA (Fig. 4) dramatically induced the expression of shati mRNA (Fig. 5a) and TNF- α mRNA (Fig. 6a) in PC12 cells. No histological or mechanical disruption was produced by transfection of the vector (Fig. 4a). Over-expression of shati (Fig. 5a), which occurs in TNF- α -immunopositive cells (Fig. 6d), potentiated DA uptake and inhibited the METH-induced decrease in DA uptake (Fig. 5b) in PC12 cells by regulating TNF- α expression (Fig. 6a), since these effects were antagonized by anti-TNF- α antibody and soluble TNF receptor I used for the neutralization of TNF- α (Fig. 6c; Barone *et al.* 1997). These findings strongly suggest that the over-expression of shati elicited by METH serves as a homeostatic mechanism that prevents behavioral sensitization and rewarding effects by attenuating the METH-induced increase in extracellular DA

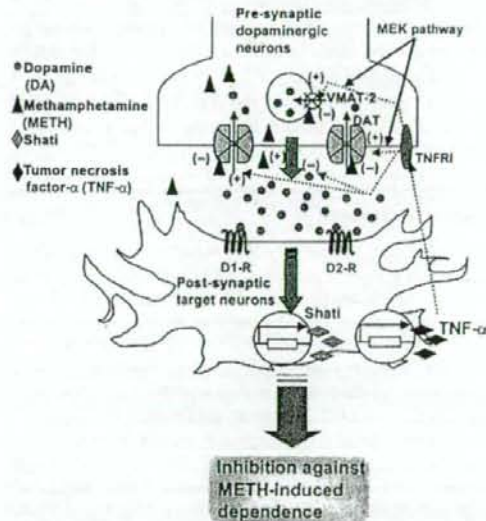


Fig. 7 Schema for regulation of TNF- α induced by shati on METH-induced DA responses. Under basal conditions, plasmalemmal DAT is involved in the reuptake of extracellular DA into the cytosol; subsequently the cytosolic DA is stored into synaptic vesicles via VMAT-2. Treatment of METH inhibits DA uptake through DA transporter and facilitates DA's release from pre-synaptic nerve terminals. METH is associated with an increase in extracellular DA levels in the brain, resulting in potentiation of the METH-induced dependence. METH induces shati and TNF- α expression in target neurons through the activation of DA receptors. TNF- α regulated by shati inhibits the METH-induced increase in extracellular DA levels in the nucleus accumbens by promoting DA uptake via MEK pathway and finally inhibits sensitization to and the rewarding effects of METH. DA: dopamine, METH: methamphetamine, TNF- α : tumor necrosis factor- α , D1-R: dopamine D1 receptor, D2-R: dopamine D2 receptor, DAT: dopamine transporter, VMAT-2: vesicular monoamine transporter-2, TNFR I: tumor necrosis factor type I receptor.

levels in the NAc through potentiation of plasmalemmal and vesicular DA uptake via induction of TNF- α expression (Fig. 7), although the mechanism by which TNF- α is regulated by shati remains to be elucidated.

Motif analyses have revealed that shati contains sequences of GNAT (Niwa *et al.* 2007a). Docking simulations with acetyl-CoA or ATP conducted using Molecular Operating Environment software reveal possible acetyl-CoA- and/or ATP-binding sites, since there is low potential energy for these interactions, in contrast with the prohibitively high energy of docking with DA, DNA or nuclear localization signals (Niwa *et al.* 2007a). These results suggest shati to have a physiological role in producing acetylcholine or the metabolic action of ATP. Accordingly, we have to investigate the mechanism by which shati regulates the production of acetylcholine or metabolic roles of ATP in subsequent studies.

In conclusion, we hypothesized that TNF- α expression induced by shati inhibits the METH-induced increase in extracellular DA levels in the NAc by promoting DA uptake and finally inhibits sensitization to and the rewarding effects of METH (Fig. 7). Targeting the shati-TNF- α system would provide a new therapeutic approach to the treatment of METH dependence.

Acknowledgments

This study was supported in part by Research Fellowships of the Japan Society for the Promotion of Science (JSPS) for Young Scientists; by Grants-in-aid for Scientific Research (B) and for Exploratory Research from the JSPS; by the 'Academic Frontier' Project for Private Universities (2007–2011) from the Ministry of Education, Culture, Sports, Science and Technology of Japan; by the International Research Project supported by the Meijo Asian Research Center (MARC); by Health and Labour Sciences Research on Regulatory Science of Pharmaceuticals and Medical Devices from the Ministry of Health, Labour and Welfare, Japan; by Research on Risk of Chemical Substances, Health and Labour Science Research Grants supported by the Ministry of Health, Labour and Welfare; by the Japan France Joint Health Research Program; and by the Uehara Foundation.

The authors are grateful to the Riken Cell Bank for the pheochromocytoma-12 (PC12) cells, and to Mrs. Nobuyoshi Hamada and Yoshiyuki Nakamura, Radioisotope Center Medical Branch, Nagoya University Graduate School of Medicine, for technical assistance.

References

Amara S. G. and Kuhar M. J. (1993) Neurotransmitter transporters: recent progress. *Annu. Rev. Neurosci.* **16**, 73–93.
 Barone F. C., Arvin B., White R. F., Miller A., Webb C. L., Willette R. N., Lysko P. G. and Feuerstein G. Z. (1997) TNF- α . A mediator of focal ischemic brain injury. *Stroke* **28**, 1233–1244.
 Baud V. and Karin K. (2001) Signal transduction by tumor necrosis factor and its relatives. *Trends Cell Biol.* **11**, 372–377. Review.

Boka G., Anglade P., Wallach D., Javoy-Agid F., Agid Y. and Hirsch E. C. (1994) Immunocytochemical analysis of tumor necrosis factor and its receptors in Parkinson's disease. *Neurosci. Lett.* **172**, 151–154.
 Cen X., Nitta A., Ibi D., Zhao Y., Niwa M., Taguchi K., Hamada M., Ito Y., Ito Y., Wang L. and Nabeshima T. (2008) Identification of piccolo as a regulator of behavioral plasticity and dopamine transporter internalization. *Mol. Psychiatr.* **13**, 451–463.
 Chen N. H., Reith M. E. and Quick M. W. (2004) Synaptic uptake and beyond: the sodium- and chloride-dependent neurotransmitter transporter family SLC6. *Pflugers Arch.* **447**, 519–531. Review.
 Devin A., Lin Y. and Liu Z. G. (2003) The role of the death-domain kinase RIP in tumour-necrosis-factor-induced activation of mitogen-activated protein kinases. *EMBO J.* **22**, 623–627.
 Finberg J. P. and Youdim M. B. (1983) Selective MAO A and B inhibitors: their mechanism of action and pharmacology. *Neuropharmacology* **22**, 441–446. Review.
 Fog J. U., Khoshbouei H., Holy M. *et al.* (2006) Calmodulin kinase II interacts with the dopamine transporter C terminus to regulate amphetamine-induced reverse transport. *Neuron* **51**, 417–429.
 Fornai F., Lenzi P., Lazzeri G., Ferrucci M., Fulceri F., Giorgi F. S., Falleni A., Ruggieri S. and Paparelli A. (2007) Fine ultrastructure and biochemistry of PC12 cells: a comparative approach to understand neurotoxicity. *Brain Res.* **1129**, 174–190.
 Franklin K. B. J. and Paxinos G. (1997) *The Mouse Brain: In Stereotaxic Coordinates*. Academic Press, San Diego.
 Grace A. A. (1995) The tonic/phasic model of dopamine system regulation: its relevance for understanding how stimulant abuse can alter basal ganglia function. *Drug Alcohol Depend.* **37**, 111–129. Review.
 Greene L. A. and Rein G. (1978) Short-term regulation of catecholamine biosynthesis in a nerve growth factor responsive clonal line of rat pheochromocytoma cells. *J. Neurochem.* **30**, 549–555.
 Guha M., Bai W., Nadler J. L. and Natarajan R. (2000) Molecular mechanisms of tumor necrosis factor α gene expression in monocytic cells via hyperglycemia-induced oxidant stress-dependent and -independent pathways. *J. Biol. Chem.* **275**, 17728–17739.
 Horn A. S. (1990) Dopamine uptake: a review of progress in the last decade. *Prog. Neurobiol.* **34**, 387–400. review.
 Hsu H., Xiong J. and Goeddel D. V. (1995) The TNF receptor 1-associated protein TRADD signals cell death and NF- κ B activation. *Cell* **81**, 495–504.
 Hyman S. E. (1996) Addiction to cocaine and amphetamine. *Neuron* **16**, 901–904.
 Jones S. R., Gainetdinov R. R., Jaber M., Giros B., Wightman R. M. and Caron M. G. (1998) Profound neuronal plasticity in response to inactivation of the dopamine transporter. *Proc. Natl Acad. Sci. USA* **95**, 4029–4034.
 Koob G. F. (1992) Drugs of abuse: anatomy, pharmacology and function of reward pathways. *Trends Pharmacol. Sci.* **13**, 177–184.
 Koob G. F., Sanna P. P. and Bloom F. E. (1998) Neuroscience of addiction. *Neuron* **21**, 467–476.
 Loder M. K. and Melikian H. E. (2003) The dopamine transporter constitutively internalizes and recycles in a protein kinase C-regulated manner in stably transfected PC12 cell lines. *J. Biol. Chem.* **278**, 22168–22174.
 Maier S. F. and Watkins L. R. (1998) Cytokines for psychologists: implications of bidirectional immune-to-brain communication for understanding behavior, mood, and cognition. *Psychol. Rev.* **105**, 83–107.
 Markey K. A., Kondo H., Shenkman L. and Goldstein M. (1980) Purification and characterization of tyrosine hydroxylase from a clonal pheochromocytoma cell line. *Mol. Pharmacol.* **17**, 79–85.

- Melikian H. E. and Buckley K. M. (1999) Membrane trafficking regulates the activity of the human dopamine transporter. *J. Neurosci.* **19**, 7699–7710.
- Morón J. A., Zakharova I., Ferrer J. V. et al. (2003) Mitogen-activated protein kinase regulates dopamine transporter surface expression and dopamine transport capacity. *J. Neurosci.* **23**, 8480–8488.
- Nakajima A., Yamada K., Nagai T. et al. (2004) Role of tumor necrosis factor- α in methamphetamine-induced drug dependence and neurotoxicity. *J. Neurosci.* **24**, 2212–2225.
- Nestler E. J. (2001) Molecular basis of long-term plasticity underlying addiction. *Nat. Rev. Neurosci.* **2**, 119–128.
- Niwa M., Nitta A., Mizoguchi H., Ito Y., Noda Y., Nagai T. and Nabeshima T. (2007a) A novel molecule 'shati' is involved in methamphetamine-induced hyperlocomotion, sensitization, and conditioned place preference. *J. Neurosci.* **27**, 7604–7615.
- Niwa M., Nitta A., Shen L., Noda Y. and Nabeshima T. (2007b) Involvement of glial cell line-derived neurotrophic factor in inhibitory effects of a hydrophobic dipeptide Leu-Ile on morphine-induced sensitization and rewarding effects. *Behav. Brain Res.* **179**, 167–171.
- Niwa M., Nitta A., Yamada K. and Nabeshima T. (2007c) The roles of glial cell line-derived neurotrophic factor, tumor necrosis factor- α , and an inducer of these factors in drug dependence. *J. Pharmacol. Sci.* **104**, 116–121.
- Niwa M., Nitta A., Yamada Y., Nakajima A., Saito K., Seishima M., Noda Y. and Nabeshima T. (2007d) Tumor necrosis factor- α and its inducer inhibit morphine-induced rewarding effects and sensitization. *Biol. Psychiatry* **62**, 658–668.
- Niwa M., Nitta A., Yamada Y., Nakajima A., Saito K., Seishima M., Shen L., Noda Y., Furukawa S. and Nabeshima T. (2007e) An inducer for glial cell line-derived neurotrophic factor and tumor necrosis factor- α protects against methamphetamine-induced rewarding effects and sensitization. *Biol. Psychiatry* **61**, 890–901.
- Niwa M., Yan Y. and Nabeshima T. (2008) Genes and molecules that can potentiate or attenuate psychostimulant dependence: relevance of data from animal models to human addiction. *Ann. NY Acad. Sci.* **1141**, 76–95.
- Rahman I. and MacNee W. (2000) Regulation of redox glutathione levels and gene transcription in lung inflammation: therapeutic approaches. *Free Radic. Biol. Med.* **28**, 1405–1420.
- Rawson R. A., Gonzales R. and Brethen P. (2002) Treatment of methamphetamine use disorders: an update. *J. Subst. Abuse Treat.* **23**, 145–150. Review.
- Roda L. G., Nolan J. A., Kim S. U. and Hogue-Angeletti R. A. (1980) Isolation and characterization of chromaffin granules from a pheochromocytoma (PC 12) cell line. *Exp. Cell Res.* **128**, 103–109.
- Sampath D., Jackson G. R., Werrbach-Perez K. and Perez-Polo J. R. (1994) Effects of nerve growth factor on glutathione peroxidase and catalase in PC12 cells. *J. Neurochem.* **62**, 2476–2479.
- Self D. W. and Nestler E. J. (1995) Molecular mechanisms of drug reinforcement and addiction. *Annu. Rev. Neurosci.* **18**, 463–495. Review.
- Sulzer D., Sonders M. S., Poulsen N. W. and Galli A. (2005) Mechanisms of neurotransmitter release by amphetamines: a review. *Prog. Neurobiol.* **75**, 406–433.
- Tischler A. S. (2002) Chromaffin cells as models of endocrine cells and neurons. *Ann. NY Acad. Sci.* **971**, 366–370. Review.
- Torres G. E., Gainetdinov R. R. and Caron M. G. (2003) Plasma membrane monoamine transporters: structure, regulation and function. *Nat. Rev. Neurosci.* **4**, 13–25. Review.
- Vaccaro K. K., Liang B. T., Perelle B. A. and Perlman R. L. (1980) Tyrosine 3-monoxygenase regulates catecholamine synthesis in pheochromocytoma cells. *J. Biol. Chem.* **255**, 6539–6541.
- Vassalli P. (1992) The pathophysiology of tumor necrosis factors. *Annu. Rev. Immunol.* **10**, 411–452. Review.
- van Vliet C., Bukeczynska P. E., Puryer M. A., Sadek C. M., Shields B. J., Tremblay M. L. and Tiganis T. (2005) Selective regulation of tumor necrosis factor-induced Erk signaling by Src family kinases and the T cell protein tyrosine phosphatase. *Nat. Immunol.* **6**, 253–260.
- Wada R., Tiffi C. J. and Proia R. L. (2000) Microglial activation precedes acute neurodegeneration in Sandhoff disease and is suppressed by bone marrow transplantation. *Proc. Natl Acad. Sci. USA* **97**, 10954–10959.
- Wise R. A. (1996) Neurobiology of addiction. *Curr. Opin. Neurobiol.* **6**, 243–251.
- Youdim M. B. (1991) PC12 cells as a window for the differentiation of neural crest into adrenergic nerve ending and adrenal medulla. *J. Neural Transm. Suppl.* **34**, 61–67.



ELSEVIER

Journal of Neuroimmunology 194 (2008) 54–61

Journal of
Neuroimmunology

www.elsevier.com/locate/jneuroim

Production and functions of IL-17 in microglia

Jun Kawanokuchi^a, Kouki Shimizu^a, Atsumi Nitta^b, Kiyofumi Yamada^b, Tetsuya Mizuno^a,
Hideyuki Takeuchi^a, Akio Suzumura^{a,*}

^a Department of Neuroimmunology, Research Institute of Environmental Medicine, Nagoya University, Furo-cho, Chikusa-ku, Nagoya 464-8601, Japan

^b Department of Neuropsychopharmacology and Hospital Pharmacy, Nagoya University Graduate School of Medicine Showa-ku, Nagoya 466-8560, Japan

Received 26 July 2007; received in revised form 16 November 2007; accepted 19 November 2007

Abstract

Interleukin (IL)-17-producing helper T cells may play a pivotal role in the pathogenesis of multiple sclerosis. Here, we examined the effects of IL-17 on microglia, which are known to be critically involved in multiple sclerosis. Treatment with IL-17 upregulated the microglial production of IL-6, macrophage inflammatory protein-2, nitric oxide, adhesion molecules, and neurotrophic factors. We also found that IL-17 was produced by microglia in response to IL-23 or IL-1 β . Because microglia produce IL-1 β and IL-23, these cytokines may act in an autocrine manner to induce IL-17 expression in microglia, and thereby contribute to autoimmune diseases, such as MS, in the central nervous system.

© 2007 Elsevier B.V. All rights reserved.

Keywords: Cytokine; IL-17; EAE; MS; Microglia

1. Introduction

Multiple sclerosis (MS) is a chronic inflammatory demyelinating disorder that affects the central nervous system (CNS). Although the etiology of MS is not fully understood, T helper 1 (Th1) cells and the cytokines that they produce are thought to play a role in the development of MS. Recently, interleukin (IL)-17 producing helper T (Th17) cells play important roles in the induction of autoimmune diseases including MS and the corresponding animal model—experimental autoimmune encephalomyelitis (EAE) (Hofstetter et al., 2005; Ishizu et al., 2005; Iwakura and Ishigame, 2006). It has been shown that IL-17 mRNA levels are high in both the cerebrospinal fluid and plaques of MS patients (Matusevicius et al., 1999; Lock et al., 2003). IL-17 is a T cell-derived proinflammatory molecule that stimulates epithelial, endothelial, and fibroblastic cells to produce other inflammatory cytokines and

chemokines, including IL-6, macrophage inflammatory protein (MIP)-2, granulocyte-colony stimulating factor (G-CSF), and monocyte chemoattractant protein (MCP)-1 (Aggarwal and Gurney, 2002; Yao et al., 1995; Kennedy et al., 1996; Fossiez et al., 1996; Linden et al., 2000; Cai et al., 1998; Jovanovic et al., 1998; Laan et al., 1999). IL-17 also synergizes with other cytokines such as tumor necrosis factor (TNF) α and IL-1 β to further induce chemokine expression (Jovanovic et al., 1998; Chabaud et al., 1998). Although the precise mechanisms that control Th17 cell development have yet to be elucidated, Th17 cells are thought to develop from naïve T helper (Th0) cells via a pathway that is different than the pathways that lead to the development of Th1 and Th2 cells. In the absence of interferon (IFN) γ and IL-4, IL-23 has been shown to maintaining Th17 phenotype in a manner that is not dependent on the transcription factors STAT1, T-bet, STAT4, and STAT6 (Aggarwal et al., 2003; Harrington et al., 2005; Park et al., 2005; Bettelli et al., 2006). Interestingly, a recent study revealed that IL-27 is a critical regulator of IL-17 production. IL-27 receptor-deficient mice were found to generate more IL-17-producing T helper cells and were hypersusceptible to EAE, suggesting that IL-27 negatively regulates the development of Th17 cells (Batten et al., 2006).

* Corresponding author. Department of Neuroimmunology, Research Institute of Environmental Medicine, Nagoya University, Furo-cho, Chikusa-ku, Nagoya 464-8601, Japan. Tel.: +81 52 789 3881; fax: +81 52 789 3885.

E-mail address: suzumura@riem.nagoya-u.ac.jp (A. Suzumura).